DETERMINING THE SPATIAL VARIATIONS OF EVAPOTRANSPIRATION RATES IN A SEMIARID REGION

Wendy Sorour

(2088247)

A research report submitted, in partial fulfillment of the requirements for the degree of Master of Science in Geographical Information Systems and Remote Sensing, to the School of Geography, Archaeology & Environmental Studies, in the Faculty of Science at the University of the Witwatersrand, Johannesburg, South Africa.

Supervisor: Dr Cletah Shoko
07 June 2024

Plagiarism Declaration

I declare that this Research Report is my own, unaided work. This Research Report is being submitted for the Degree of Master of Science in Geographical Information Systems and Remote Sensing at the University of the Witwatersrand, Johannesburg. It has not been submitted before for any examination or degree at any other University.

Student Name: Wendy Sorour

Student Number: 2088247

Signature: 

Date: 07 June 2024

Abstract

Evapotranspiration (ET) is one of the biggest ways in which water is transferred from water resources into the atmosphere as water vapor and understanding its variations is important for water resource management. This study determined land use land cover (LULC)-based ET and the influence of climatic events in Western Cape. Landsat 8, Surface Energy Balance System, Support Vector Machine, humidity, wind speed, surface pressure, temperature, and sunshine hours were used, during El Nino in 2015-2016, normal year in 2019-2020, and La Nina in 2020-2021. Median ET was calculated for each LULC type to determine their effect on ET. Climatic events increased ET compared to the normal year and increasing temperatures and rainfall during EL Nino and La Nina years respectively were the main drivers. Water had the lowest ET, and agricultural land had the highest. The results of this study can be used to create better water resource management plans.

Keywords: Climatic events, El Nino, Evapotranspiration, La Nina, LULC, SEBS, and Western Cape.

Dedication

I would like to dedicate my paper to my husband. He has been my rock, constant support, and strongest believer since the start of university and if it was not for him, I would not have seen my degree this far. I would like to thank my husband for always being there for me and always encouraging me through my many stressful moments, believing I could get through anything even when I thought it was impossible.

Acknowledgment

Most importantly, I am thankful to my supervisor, Dr Cletah Shoko, for her continuous guidance and support throughout my research. Her continuous moral support, detailed feedback, and record-response time helped me work through all my queries and produce a project on time that I can be proud of.

I am thankful to my husband for all his moral support throughout this journey, pushing me through all the ups and downs and encouraging me to always do my best and stay positive no matter the challenge. I appreciate my parents and my mother-in-law for supporting me through my continuous years of studying, allowing me to get this far in my degree, and always believing in me. Lastly, I am thankful to my friends and family for all the extra support, and for always being willing to listen to my rants and support me through my many stressful moments throughout the year.

Table of Contents

List of Figures

List of Tables

List of Acronyms

Evapotranspiration	ET
El Nino-Southern Oscillation	ENSO
Land use land cover	LULC
Surface Energy Balance System	SEBS
Support Vector Machine	SVM
Sea surface temperatures	SST
Surface energy balance	SEB
Maximum likelihood classification	MLC
Surface Energy Balance Index	SEBI
Penman-Monteith	PM
Surface Energy Balance Algorithm over Land	SEBAL
Normalized difference vegetation index	NDVI
Integrated Land and Water Information System	ILWIS
Mapping ET at high Resolution with Internalized Calibration	METRIC
Root mean square error	RMSE
Operational Simplified Surface Energy Balance	SSEBop
Normalized difference water index	NDWI
United States Geological Survey	USGS
Near Infrared	NIR
Shortwave Infrared 1	SWIR-1
Shortwave Infrared 2	SWIR-2
Thermal Infrared 1	TIRS-1
Thermal Infrared 2	TIRS-2
Shuttle Radar Topography Mission	SRTM
Digital elevation model	DEM
Automatic Weather Stations	AWS
Land surface temperature	LST
Fractional Vegetation Cover	FVC
Global climate models	GCM
Soil and Water Assessment Tool	SWAT
National Land Cover	NLC
Random Forest	RF

CHAPTER ONE: GENERAL INTRODUCTION

1.1 Introduction

Water resource management and planning are very important in semi-arid and arid regions as water is a scarce resource in these areas (Rwasoka *et al.,* 2011). Understanding all aspects of the hydrological processes also helps us create better water resource management plans (Gibson *et al.,* 2011). Evapotranspiration (ET) refers to the combined transfer of water from a water or vegetation source to the atmosphere as water is converted by heat into vapor (Elhag *et al.,* 2011). This phenomenon is said to be one of the major ways in which water is transferred within the water budget from the ground to the atmosphere within semiarid and arid regions in Southern Africa (Shoko *et al.,* 2015a). ET is the second largest contributor to the water balance after precipitation making it a very important factor to analyze and understand, especially in regions where water scarcity issues exist (Shoko *et al.,* 2015a). In previous studies, it has been shown that understanding the ET rate specifically can help with water use estimation as well as water allocation and usage planning (Gibson *et al.,* 2013).

Climatic events affect the amount of rainfall that any area receives. Any changes that occur within the climatic system cause changes in the water system. These include that some hydrological extremes become more extreme like increasing vulnerable areas and hot spots (Kundzewicz, 2008). Within arid and semi-arid regions, any variations in temperature and precipitation, which are often caused by climatic events, cause significant changes in the water system including the ET rate. These climatic events, like climate change, can increase or decrease the dry conditions which will increase or decrease the ET (Huo *et al.,* 2013). For example, climate change affecting the temperature and precipitation is seen all over the world with increasing temperatures in areas like the USA (Fan *et al.,* 2016), Egypt (Khalil, 2013), and Iran (Valipour *et al.,* 2017). These increasing temperatures affect the ET rates in all these areas which are just a few examples from all around the world (Khalil, 2013; Fan *et al.,* 2016; Valipour *et al.,* 2017).

A specific climate phenomenon known as El Nino-Southern Oscillation (ENSO) has a major effect on climate on tropical weather patterns on a global scale (Shikwambana *et al.,* 2023). This is because these events cause changes in the Sea surface temperatures (SST) of the tropical Pacific which has a global impact on the climate. There are 3 different phases, the La Nina

phase when the SST is slightly warmer than normal, the El Nino phase when the SST is slightly cooler than normal, and the neutral phase (Shikwambana *et al.,* 2023).

These phases of the ENSO climatic events affect the climate worldwide in different ways. Some areas experience droughts while others experience flooding. The El Nino events in most countries cause a decrease in precipitation. Severe drought is associated with countries like Mexico, Honduras, Caribbean countries, African countries (including Nigeria, Mali, Sudan), and Mozambique. South and Southeast Asia, Australia, and Indonesia also are noticeably drier places during the EL Nino event (Generoso *et al.,* 2020). In contrast, the La Nina event usually has the opposite effect to the La Nina event, with most countries experiencing wetter than normal conditions. Very heavy rain and flooding are observed during this event in countries such as Malaysia, Australia, the Philippines, and Indonesia. However, in contrast, Chile, East Africa, and Argentina experienced drought during the La Nina event (Generoso *et al.,* 2020). The increase and decrease of rainfall and temperature in these different phases affect the ET rate due to the nature of ET (Huo *et al.,* 2013; Generoso *et al.,* 2020).

Many different methods have been developed to better understand, calculate, and estimate the ET rates at various scales (Elhag *et al.,* 2011; Hassan *et al.,* 2018; Rocha *et al.,* 2023). These various methods include those that use meteorological data and those that are based on remotely sensed data integrated with meteorological data. Methods that use meteorological data only rely solely on data that is available from weather stations in the area (Sirmohammadi-Aliakbarkhani and Saberali, 2020). However, the calculations when using solely meteorological data can be quite complicated and one only knows the weather conditions at the point of the weather station. This leads to making large area predictions based on the data from a single point which can cause over-generalization depending on the variation in the climate within the area between weather stations (Sirmohammadi-Aliakbarkhani and Saberali, 2020).

Due to the limitations of meteorologically only based methods, remote sensing in conjunction with meteorological data methods was developed and different models were created. These methods include Water Balance Method, Water-Carbon Linkage Method, Empirical Models, Surface Energy Balance Methods (SEB), etc. (Zhang *et al.*, 2016). Using remote sensing techniques in conjunction with meteorological data to calculate ET has many advantages. These include being able to calculate the ET rates over a bigger study area in a less time-

consuming manner than any other method and being able to do continuous monitoring over a long time due to the availability of many different satellite images for many years and meteorological recording of data from various weather stations for various years (Gibson *et al.,* 2013). Another advantage of using remote sensing methods is that one can determine the different ET rates for different LULC types which helps one better understand where ET is occurring most over a large area of different types of land (Rwasoka *et al.,* 2011; Shoko *et al.,* 2015a).

1.2 Problem Statement

Water resource management is highly important in the Western Cape as this is a province that struggles with drought (Muller, 2018). ET is a big contributing factor to water that is available as a water resource on the ground being lost to the atmosphere (Shoko *et al.,* 2015b). Remote sensing data integrated with meteorological data to determine ET using SEBS models has been shown to create better estimates of bigger study areas and the ability to perform long-term continuous monitoring (Gibson *et al.,* 2013; Shoko *et al.,* 2015b; Rwasoke *et al.,* 2011). In the Western Cape, there have been a few studies done on various aspects of water resource management (Dzikiti *et al.,* 2013; Jovanovic *et al.,* 2014; Veste *et al.,* 2020; Bhaga *et al.,* 2021). However, none of these studies have determined the ET rates of a catchment area in the Western Cape for different LULC types for the different seasons and the effects of the El Nino and La Nina climate events on ET.

1.3 Aim

To determine the spatial and temporal variations of ET for different LULC types and the influence of certain climatic phenomena in a semi-arid region of the Western Cape.

1.4 Specific Objectives

1. To determine the seasonal variations in ET for the La Nina year of 2020/2021, the El Nino year of 2015/2016, and the Normal year of 2019/2020.
2. To assess the LULC variations within the study area for the summer and winter seasons for La Nina year 2020/2021 and El Nino year 2015/2016.
3. To determine ET variations for the different LULC types during the La Nina year of 2020/2021, the El Nino year of 2015/2016, and the Normal year of 2019/2020.

1.5 Structure of the Research Report

This report consists of five chapters. The first chapter is the general introduction where the concept of ET, land use land cover, and climatic events are introduced and the problem statement, aims, and objectives of the study are stated. The second chapter consists of the literature review which includes a review of various literature relating to the different concepts and methods used in this study. The third chapter is the methodology chapter where the study site is explained and the methods used throughout the study are shown in a summarized workflow, followed by a detailed explanation. The fourth chapter is the results section where all the results of the study are represented and explained in various figures and tables. The fifth chapter is the final chapter, which includes a discussion of the results comparing them to the results of other studies, the limitations of the study, concluding statements, and recommendations for future studies.

CHAPTER TWO: LITERATURE REVIEW

2.1 Introduction

This chapter focuses on presenting and analyzing the different literature that is available with regards to the importance of ET, the extreme climatic events characteristics and relevance to ET, different land use land cover classifications, the different methods that are available to estimate the ET, and specific focus on the SEBS model that was chosen for this study. The studies that were chosen were from across the globe with a specific focus on Africa that were possible and relevant.

2.2 The importance of understanding ET for water management planning

ET is one of the biggest ways in which water available as a water resource is lost to the atmosphere in semiarid and arid regions through the transformation of water to water-vapor by heat (Rwasoka *et al.,* 2011; Rocha *et al.,* 2023). Being able to understand the rate at which this water is lost will help create better water resource management plans especially in the agricultural sector where managing irrigation quantities would greatly decrease the amount of water lost (Rwasoka *et al.,* 2011; Elkatoury *et al.,* 2020).

Within South Africa, it is particularly important to understand the ET rates as one can create a much better water resource management plan if one understands all the aspects of the occurrences that affect the amount of water available for use (Gibson *et al.,* 2011). Better resource management plans are important to have for the study area chosen as there is a big agricultural sector and with this being a winter rainfall area, a lot of water is lost through ET in the summer that is not replenished through precipitation within these months (Jovanovic *et al.,* 2014).

2.3 An overview of climate change and extreme events

Global warming and climate change are a reality in today's world where the increasing human population, land use land cover changes, environmental pollution, urbanization, etc. are constantly creating more pressure on the environment, negatively impacting the climate (Kundzewicz, 2008). The temperature increase seen around the world since the mid-20th century is mostly equated to the increase in greenhouse gas concentration in the atmosphere. Specifically with regards to the hydrological cycle, the amount of freshwater that is available has been seen to be decreasing due to an increase in temperature as more water is evaporating

(Kundzewicz, 2008). It has been predicted that the number of consecutive days without rainfall and the frequency of the occurrence of heavy rainfall are predicted to increase in the future (Kundzewicz, 2008)

One of these climatic events that are becoming more extreme is the ENSO stage. ENSO is a climatic phenomenon that occurs due to changes in the Pacific SST which result in global changes in the atmospheric conditions affecting the precipitation and temperature across the world (Harduth and Fitchett, 2020; Shikwambana *et al.,* 2023). ENSO climatic events are said to be strong drivers of climate variability especially in terms of the effects on agricultural production (Philippon *et al.,* 2011; Sazib *et al.,* 2020). There are some suggestions that the occurrence and characteristics of these ENSO events are affected by global warming. For example, most of the strong El Nino events that have occurred in history have occurred during the past half century, in 1982-83, 199798, and 2015-16 (Marjani *et al.,* 2019). There has also been a strong increase in La Nina events in the past half-century, including 1988-89, 1999-2000, 2007-08, and 2010-11. This shows that there might be an increase in ENSO events with global warming (Marjani *et al.,* 2019). Climate change has also influenced the frequency of the different stages of the La Nina and El Nino events, with more El Nino events occurring in the late 20th century than La Nina events. If this trend continues this will harm many countries as an increase in El Nino events increases in drought stages occurring within many different countries across the globe (Mason *et al.,* 2001).

The global effect of these events is different depending on the geographic location of the country and the seasonal patterns experienced in a normal year. Grimm *et al.* (2000) studied the effect of El Nino and La Nina events on southern South America regions. There were ten El Nino and eight La Nina events used between 1956-92 and it was discovered that on average the El Nino (La Nina) event results in a lower (higher) than median precipitation for the year before the event continuing into the March of the year of the event (Grimm *et al.,* 2000). In Europe, through studying the ENSO stages that occurred in the 18th and 19th centuries, Bronnimann *et al.* (2007) found that the effect of El Nino caused negative temperature changes in northeastern Europe, positive temperature changes in Turkey, negative precipitation changes in Norway and the southeastern Mediterranean area and positive precipitation changes around 45°N. In most areas, the La Nina event caused a close to symmetrical but opposite response in the temperature and precipitation changes in these areas in Europe (Bronnimann *et al.,* 2007).

Specifically, the strong ENSO phases of 2020/2021 and 2015/2016 were found to have a great impact on the climate of South Africa which greatly affected many different aspects such as wildfires, agriculture, extreme events like flooding and drought as well as seasonal variation in rainfall, wind speed, wind direction, etc. (Sazib e*t al.*, 2020; Shikwambana and Kganyago, 2023; Shikwambana *et al.*, 2023). The same strong El Nino event in 2015/2016 caused strong vegetation stress in the ecosystems of eastern Australia, South America, and Southeast Asia which negatively impacted the water resources and agriculture in these countries (Kogan and Guo, 2017).

Philippon *et al.* (2011) performed a study on the effects of the La Nina and El Nino ENSO stages on the winter rainfall area in South Africa and they found that during the El Nino event, the rain-bearing systems are located further north, larger, and deeper in extent meaning that more rainfall/increased wet spells are experienced during the El Nino event. On the other hand, during the La Nina event, the rain-bearing systems were located further south with smaller and thinner extents resulting in less rainfall and shorter, less frequent wet spells (Philippon *et al.*, 2011). With regards to wind speed during these events, it has been found that the wind speed is weaker (stronger) during El Nino (La Nina) events which leads to the changes in the sea surface temperature associated with these events (Rouault *et al.*, 2010).

2.4 Land use land cover classification from remote sensing

ET from land surfaces is responsible for about 65% of continental precipitation and utilizes around half of the solar radiation that the land surface absorbs (Odongo *et al.*, 2019). This highlights how LULC has an important linkage to ET as climate and land change are two major factors that affect ET. The changing of climate is also greatly affected by the LULC change which in turn is greatly affecting the hydrological cycle in many ways, especially ET rates. Vegetation specifically, has strong effects on the various aspects of the hydrological cycle including ET, runoff, and infiltration of water to the water table (Odongo *et al.*, 2019). Understanding in more depth the extent to which the different LULC types affect the ET rate is important to be able to create better water management plans as the LULC types are changing.

Image classification in general is used in a variety of fields including urban planning, agriculture, coastal and ocean monitoring, forestry, etc. (Sisodia *et al.*, 2014). The general concept of image classification in remote sensing involves grouping a set of pixels into a finite number of individual classes based on the values of the pixels. The classifications are then generally represented in the form of a thematic map which shows classes like vegetation, water bodies, land use, etc. much like what will be done in this study (Sisodia *et al.*, 2014).

Image classification in general consists of two main types, classifications that are either pixel-based or object-based (Li *et al.*, 2014; Sisodia *et al.*, 2014). These classification methods have been continuously developing since the 1980s for the pixel-based and the 1990s for the object-based analysis (Li *et al.*, 2014). Pixel-based classification can be further divided into supervised (ISODATA and k-means) and unsupervised techniques (maximum likelihood (MLC), SVM, random forest (RF), etc.) (Li *et al.*, 2014; Sisodia *et al.*, 2014).

With regards to unsupervised classification, little to no knowledge of the study area before the identification of different classes is required. The unsupervised classification just calculates the minimum distance between the object mean and the class mean of every possible class and keeps doing this until the means remain constant and then the object is assigned to the relative class (Sisodia *et al.*, 2014). Due to the characteristics of the unsupervised classification, the results of the classification can result in the objects of the entire classification having no obvious separation and many misclassifications occurring (Li *et al.*, 2020). A study by Mohad *et al.* (2009) compared the unsupervised and supervised classification methods by determining the LULC classes of the Ayer Hitam Forest Reserve located in Puchong, Selangor using SPOT 5 imagery and the MLC (unsupervised) and ISODATA (supervised) classification methods. Mohd *et al.* (2009) found the unsupervised classification to be more noisy and less accurate than the supervised classification.

The supervised classification method, however, requires one to create training sites and assign specific LULC classes. This input information helps train the classifier to determine the boundaries of the decisions made in the classification feature space (Sisodia *et al.*, 2014). The unsupervised classification might be quicker and more automated than the supervised classification but when there are similar or the same reflectance between classes (like between bare land and built-up areas) the unsupervised classification provides less accuracy due to the problem of mixed pixels (Li *et al.*, 2014; Sisodia *et al.*, 2014). So, when more specific LULC

types need to be identified and classified, increased accuracy is needed and more prior knowledge about the study area is known, it is preferred to use a supervised classification method.

The supervised classification method also includes a variety of different methods that can be used to classify an image. These various methods include RF, SVM, MLC, etc. Most of these methods work relatively accurately overall and studies have been done to determine which method is best to use depending on the characteristics of the data. In three different studies (Nitze *et al.,* 2012; Noi and Kappas 2017; Sheymousa *et al.,* 2020), the SVM outperformed the RF, k-nearest neighbors, and artificial neural networks. However, in general, all the classifiers had at least over 85% accuracy rate. Sheymousa *et al.,* (2020) also found that when the images were at a medium resolution (between 10m to 100m spatial resolution), the SVM outperformed the RF technique. This indicates the potential of using SVM when working with Landsat images with 30m spatial resolution. Noi and Kappas (2017) found that SVM showed a lower sensitivity to training sample size over RF, whereas Nitze *et al.* (2012) found that the SVM is more robust and accurate than the other classification methods.

Although pixel-based classifications are used widely in various studies, they also have their disadvantages. The pixel-based classification methods become inaccurate when the size of an object is smaller than a pixel, resulting in one pixel containing different land use land cover types causing a mixed pixel effect (Li *et al.,* 2014; Sisodia *et al.,* 2014). Another big challenge for this type of classification is the classification of rocks versus shadows, water and blue ice, and snow and ice (Jawak *et al.,* 2015). This is where the object-based classifications can be used, depending on the requirements of your study. If misclassifications are required to not occur in these different classes or small objects are within pixels, object-based classification would be the better method to use to avoid the disadvantages of pixel-based classifications (Jawak *et al.,* 2015).

Using remote sensing to perform LULC change detection has been a common practice for many years with many studies performing comparisons as to which method is most accurate and common. A study by Chughtai *et al.* (2021) was reviewed to determine which LULC change detection method is most accurate and common. The MLC method was found to be the most accurate and commonly used technique from past to present studies in all regions when compared to the other techniques (Chughtai *et al.,* 2021). Esmail *et al.* (2016) found that the

SVM classification performs accurately (97% to 100% overall accuracy) in coastal areas along the Nile Delta to determine land change detection using Landsat images from 1987 to 2015. Using Landsat images from 1990 and 2010, Rawat and Kumar (2015) showed that the MLC technique can accurately determine change detection in the Hawalbagh block of Almora district, India. The MLC performed with 90.29% and 90.13% overall accuracy in this region. These studies show that although the MLC classification is the most popular and accurate classification method in all regions, other classification methods are also accurate, and considering the study area characteristics when choosing a classification method is important (Chughtai *et al.*, 2021).

2.5 Approaches to ET estimation

There are various ways in which energy balance methods are used in remote sensing. When these models are used, physical modules and empirical relationships are determined from meteorological and remotely sensed data (Gibson *et al.*, 2011). The foundation of the SEB approach using remote sensing was based on the Surface Energy Balance Index (SEBI) which predicts ET from each pixel using the energy balance equation: $\lambda E = R_n - G_0 - H$, where λE = turbulent latent heat flux, R_n is net radiation, G_0 = soil heat flux and H = sensible heat flux (Su, 2002).

There are also field-based measurements of fluxes which are used to estimate ET. These are scintillometers, the Bowen ratio, eddy covariance systems, the Penman-Monteith (PM) equation, etc. (Ali *et al.*, 2009; Gibson *et al.*, 2013; Gwate *et al.*, 2018a). Many studies have been carried out to determine the accuracy of these field-based measurement techniques (Ali *et al.*,2009; Gwate *et al.*, 2018a). These studies have found that micrometeorological techniques such as the scintillometer are very costly and therefore have not been widely used but are at most used to validate models at a local scale (Gwate *et al.*, 2018a). The PM equation, however, is one of the most robust equations essentially driven by collecting routine meteorological data from physical weather stations (Ali *et al.*, 2009; Gwate *et al.*, 2018a). Unfortunately, with all these field-based measurement analyses, the accuracy and availability of the measurements significantly affect the prediction of ET. Gwate *et al.* (2018a) found that if wind speed at the reference height is used for the PM equation, ET can be significantly overestimated if the reference height does not match the canopy height of the vegetation. The lack of availability of all the required field measurements for the field-based methods is a

reason that sometimes the remotely sensed methods incorporating some field measurements are used (Gibson *et al.*, 2013; Gwate *et al*., 2018a; Gwate *et al.*, 2018b).

Two of the main models that are used to estimate ET using remote sensing are the SEBS model and the Surface Energy Balance Algorithm over Land (SEBAL) model (Gibson *et al.*, 2011; Gibson *et al.*, 2013; Ma *et al.*, 2013; Abid *et al.*, 2019). Each of these models has its advantages and disadvantages. When choosing which model to use it is important to keep the model's advantages and disadvantages in mind and choose the most suitable model depending on your study area, the results you require, and the accuracy you require (Gibson *et al.*, 2011).

The SEBAL model is designed for the ET calculations at a regional level on the land surface. This model uses the interrelationships of surface reflectance, surface temperature, and normalized difference vegetation index (NDVI) together to deduce surface fluxes, and the threshold values are determined from both the wet and the dry surfaces in the study area (Gibson *et al.*, 2011). Many different studies have been done to accurately estimate the ET of various areas globally using this model (Abrishamkar and Ahmadi, 2017; Ghaderi *et al.*, 2020; Shamloo *et al.*, 2021). One of the main advantages of this model is that it requires a few variables to calculate the ET. However, unfortunately, it is an intellectually protected method that requires the developer's permission to be able to use it and this model can only be applied to a study area if both wet and dryland pixels are available (Gibson *et al.*, 2011).

The SEBS model developed by Su (2002), which is used in this study, unlike the SEBAL model, is freely available through an open-source software called Integrated Land and Water Information System (ILWIS) coded in C++ and available in BEAM coded in Java. This software can be downloaded from the University of Twente website (https://www.itc.nl/ilwis/download/ilwis33/). This makes this model much easier to gain access to for ET estimation and has made this model much more commonly used in various studies (Gibson *et al.*, 2011; Gibson *et al.*, 2013; Abid *et al.*, 2019).

The SEBS model requires three sets of information (Su, 2002). The information derived from the remote sensing images includes the land surface albedo, emissivity, temperature, fractional vegetation coverage, and the NDVI. The second set of information is the meteorological data that is often retrieved from weather stations in the study area including the temperature, humidity, air pressure, wind speed, and reference height of weather data. Finally, the downward

longwave radiation and downward solar radiation are needed which is either measured, parametrized, or an output from the model (Su, 2002). A disadvantage of this model is that it is very complex and has many inputs from several different sources and this may result in potential errors being introduced in many different stages and from the various inputs during the complex analysis (Gibson *et al.*, 2011).

2.5.1 A sample of studies done to determine ET using the SEBS Model across the globe

Table 2.1 below shows various studies that have been done using the SEBS Model to analyze the ET rates of different areas globally, over different periods and what the major findings of these various studies were. These studies found that the SEBS model determined the ET rate of various areas accurately while using different satellite imagery. The studies show that the SEBS model is diverse in its ability to accurately determine the ET rate of different areas, in different time frames, using different satellite imagery.

Table 2.1: A table representing case studies in ET estimation using a remote sensing approach.

Study Done by	**Satellite Used**	**Model Used**	**Area Studied**	**Period of Study**	**Major findings**
Elhag *et al.,* 2011	AATSR & MERIS	SEBS	Nile Delta	August 2007	Daily ET Low of 1.2 and high of 7.1 mm
Elkatoury *et al.,* 2020	Landsat 8	SEBAL, METRIC, S-SEBI	205.5 km^2 of At-Todhia Arable Farm (TAF), Saudi Arabia (KSA).	January to December 2014	Daily ET of 2.8-22.4 mm for the most accurate METRIC model
Haung *et al.,* 2015	MODIS	SEBS with NDWI	Haihe River Basin, China	24th June, 10th July, 2nd August, 3rd September 2012	Ranges from 1.5mm/day to 4.0mm/day.
Mohammadian *et al.,* 2017	Landsat 8	SEBS	Zayanderud Dam area, central Iran	1 image per year for 2013-2015	2013 – 11.2mm 2014 - 10.58mm 2015 – 8.94mm
Rwasoka *et al.,* 2011	MODIS	SEBS	Upper Manyame catchment, Zimbabwe	Nine clear sky days from 2003 to 2005	Range of 0 – 9 mm/day over all the 9 images.
Shoko *et al.,* 2015a	MODIS	SEBS	Southwestern Zimbabwe	October 2000 to October 2012	Monthly ET of 0.0 to 42.5 mm.
Shoko *et al.,* 2015b	Landsat 8 and MODIS	SEBS	uMngeni catchment, South Africa	May 2013 to April 2014	Landsat 8 (3.6mm/day) more accurate than MODIS (2.3mm/day)
Singh and Senay, 2015	Landsat 5 and 7	METRIC, SEBAL, SEBS, SSEBop	Midwestern United States	July to December 2001	Range from 0.73 mm/day to 6.52 mm/day
Zhao *et al.,* 2019	Multifunctional Transport Satellite (MTSAT)	SEBS	Haihe River Basin, China	10 days in each season from 01 January to 10 October 2010.	3-hourly average ET of 0.873 mm/d.

There have been many studies done comparing the different SEB models in determining ET (Huang *et al.,* 2015; Singh and Seney, 2015; Elkatoury *et al.,* 2020). Elkatoury *et al.* (2020) compared three SEB models (SEBAL, METRIC, and S-SEBI) in determining ET rates using one Landsat 8 image per month for the year 2014 within the Todhia Arable Farm which was in Riyadh province in Saudi Arabia. In this study, it was found that the Mapping ET at high Resolution with Internalized Calibration (METRIC) SEB model was the most accurate with a

root mean square error (RMSE) of only 1.7 mm/day. The LULC with the highest ET values was also determined, which was found to be the cultivated areas, especially during periods of high irrigation (Elkatoury *et al.,* 2020).

Another comparison of four different SEB models done in the Midwestern United States from July to December 2001 using Landsat 5 and 7 images also found the METRIC model to be slightly more accurate (Singh and Senay, 2015). The METRIC model and the Operational Simplified Surface Energy Balance (SSEBop) model were found to have an RMSE of <0.91mm/day as opposed to the SEBS model which had an RMSE of 0.66mm/day and the SEBAL model which has an RMSE of 0.43mm/day. However, Singh and Senay (2015) mentioned that each model had its limitations and advantages, and these needed to be considered depending on the requirements of the analysis being performed.

The SEBS model specifically is a very common model to be used to estimate ET due to its free access and accuracy in determining ET. This is shown through the many different studies that have used the SEBS model to accurately determine ET in various study areas (Rwasoka *et al.,* 2011; Huang *et al.,* 2015; Shoko *et al.,* 2015a; Mohammadian *et al.,* 2017; Zhao *et al.,* 2019). Shoko *et al.* (2015a) show the importance of using a SEBS model to determine the ET rates of an arid area in Matabeleland South Province in Zimbabwe using MODIS imagery. It was accurately determined that the monthly ET within this area is between 0.0 to 42.5mm. Huang *et al.* (2015) showed the accuracy of both the SEBS model with and without the use of a normalized difference water index (NDWI) image in the Haihe River Basin, China using MODIS imagery for four dates in 2012. It was determined that using the SEBS model without the NDWI was accurate but in water-stressed environments, the accuracy of the prediction was increased using the NDWI image (Huang *et al.*,2015).

Rwasoka *et al.* (2011) used the SEBS algorithm to determine which LULC types have higher ET rates in the Upper Manyame catchment of Zimbabwe using MODIS imagery for nine clear days between 2003 and 2005. They found that water bodies and open and closed broadleaved deciduous forests had high ET rates, whereas open grassland had low ET rates. Another study done using the SEBS model with Landsat 8 images compared the ET rates estimated using the SEBS model and PM equation for 3 different years in the Zayanderud Dam area in central Iran (Mohammadian *et al.*,2017). Although both methods were found to be accurate, the SEBS

model was shown to have a slightly higher accuracy in estimating the ET for this study area (Mohammadian *et al.*,2017).

The SEBS model accuracy is also shown by Zhao *et al.* (2019) in the Haihe River Basin in China using the MTSAT imagery for 10 days in each season from 01 January to 10 October 2010. Using geostationary satellite remote sensing data (MTSAT) and in-situ meteorological data, the SEBS model accurately checked against ground truth data, with an $R^2 = 0.67$ (Zhao *et al.*, 2019).

2.6 Summary of the Chapter

Many studies have been done on the various aspects of this study including the importance of ET in terms of water management planning and the importance of understanding the dynamics of ET, climatic events and their effects on the climate around the world, LULC change, and the various methods that have been developed to classify and monitor LULC over time, the various approaches that exist to determine the ET rate and the various studies that have been done using the SEBS model to accurately determine the ET of different areas around the globe. All these studies have helped to provide background information that helped determine the best method to use to achieve the objectives of this study.

Gaps were found to exist within the literature included in this literature review. There were no studies found that have been done within the catchment area to determine ET using the SEBS Model and Landsat 8 imagery. To try and ameliorate this gap, studies that were done in semi-arid regions in other Southern African countries using SEBS and Landsat 8 imagery were referred to within this review. There were also minimal studies in which Landsat 8 imagery was used with the SEBS model to determine the ET rate in semi-arid regions. It is more common that MODIS imagery is used with the SEBS model, however, the spatial resolution of Landsat 8 imagery is much higher than MODIS imagery. Therefore, a few studies were found, and their methods combined to determine the methodology used in this study. This study will start to fill the above-mentioned gaps in the available literature.

CHAPTER THREE: METHODOLOGY

3.1 Introduction

This chapter focuses on the methods used in this study to achieve the aim and objectives of the study. The study site is outlined and described in detail. Following this, the workflow summarizes the methodology and then it is expanded on in detail afterwards. The detailed description explains how the satellite images were downloaded and preprocessed, the meteorological data was retrieved and prepared, the SEBS inputs were prepared, the LULC classifications were performed, the SEBS model was run, and the accuracy assessments were performed. Ending off the chapter is an explanation of how the comparison of the ET to the meteorological data and LULC types was conducted.

3.2 Study Site

Western Cape is one of the nine provinces in South Africa on the coast with its capital being Cape Town. It is located on the southernmost edge of the African continent between the Atlantic and Indian oceans (Zwane, 2019). The province is diverse in many ways including in its topography and climate. It is the fourth largest province in South Africa as well as the province with the fourth largest population consisting of one metropolitan municipality, 24 local municipalities, and five district municipalities (Zwane, 2019).

There are roughly 3 different drainage regions within the province with many sub and quaternary catchments. The quaternary catchments chosen in this study area (Figure 3.1) were all from one sub-catchment and were chosen so that the study area was covered by one Landsat 8 image to ensure accuracy. This group of quaternary catchments covers a large portion of the agricultural area within the Western Cape Province. The area extends from roughly Banghoek Private Nature Reserve to Theewaters Nature Reserve, covering an area of 6904,87 km^2. The drainage basin shapefile was retrieved from the government website (https://www.dws.gov.za/iwqs/wms/data/000key2data.asp).

The Western Cape has a Mediterranean climate with cool and wet winters from May to August and warm but dry summers from November to March (Bhaga *et al.*, 2021). The area of study within the Western Cape is within the Frontal rain zone in South Africa meaning it receives its rain in Winter with an annual rainfall of about 450mm (Jovanovic *et al.*, 2014). This does result in a very high mean potential annual evaporation rate of about 2150 mm which results in 70%

of the time the daily evaporation rate being greater than the rainfall amount (Jovanovic *et al.,* 2014). The dry season ranges from October to June which includes the spring, summer, and autumn seasons (Western Cape Government, 2014). The autumn and spring seasons are in-between seasons where the temperatures are from mid-teens to mid-twenties. The summer and autumn seasons are very popular for national and international visitors (Zwane, 2019).

The hottest month within the study area is February which has an average temperature of 23°C and the coldest month is July which has an average temperature of 12°C. In summer temperatures often exceed 30°C (Jovanovic *et al.,* 2014). However, in general, because of the effects of the Indian and Atlantic oceans on the Western Cape Province as a whole, the inland, and coastal temperatures differ substantially over short distances, and often micro and macro climates are created as a result (Western Cape Government, 2014). The topography does not play a major role in this climate as in general, it is mostly flat with gentle rolling elevation change within the countryside (Western Cape Government, 2014).

The fact that the daily evaporation rate is greater than the daily rainfall 70% of the time highlights how important understanding ET is as more water is being lost to the atmosphere than is being returned through precipitation (Jovanovic *et al.,* 2014). Having higher temperatures in the dry season also results in more ET than rainfall throughout most of this season once again highlighting the importance of understanding just how much water is being lost to the atmosphere through ET (Jovanovic *et al.,* 2014). Between the years 2016 to 2018, the Cape Town area was hit by a severe drought that led to water restrictions (Muller, 2018). A cause of this was the strong El Nino event during 2015/2016. Therefore, being able to understand the effects of these events on ET will help prevent the severe consequences of droughts. This will also be important for areas like Stellenbosch, which is a wine area where lots of crops are irrigated and lots of water is used.

Within this province, agriculture is one of the biggest land uses accounting for 12% of the total agriculture in the country (DEADP, 2011; Talanow *et al.,* 2021). Other land uses of this province include informal settlements, urban areas, mining, forestry, conservation and biodiversity, and invasive and alien plants (DEADP, 2011). Due to this province being so agricultural-focused, understanding the climate is important for management plans. Climate

change has occurred within the Western Cape with the mean annual temperature rising around 1°C over the last 50 years, increased flooding, heat waves, and droughts (Talanow *et al.*, 2021).

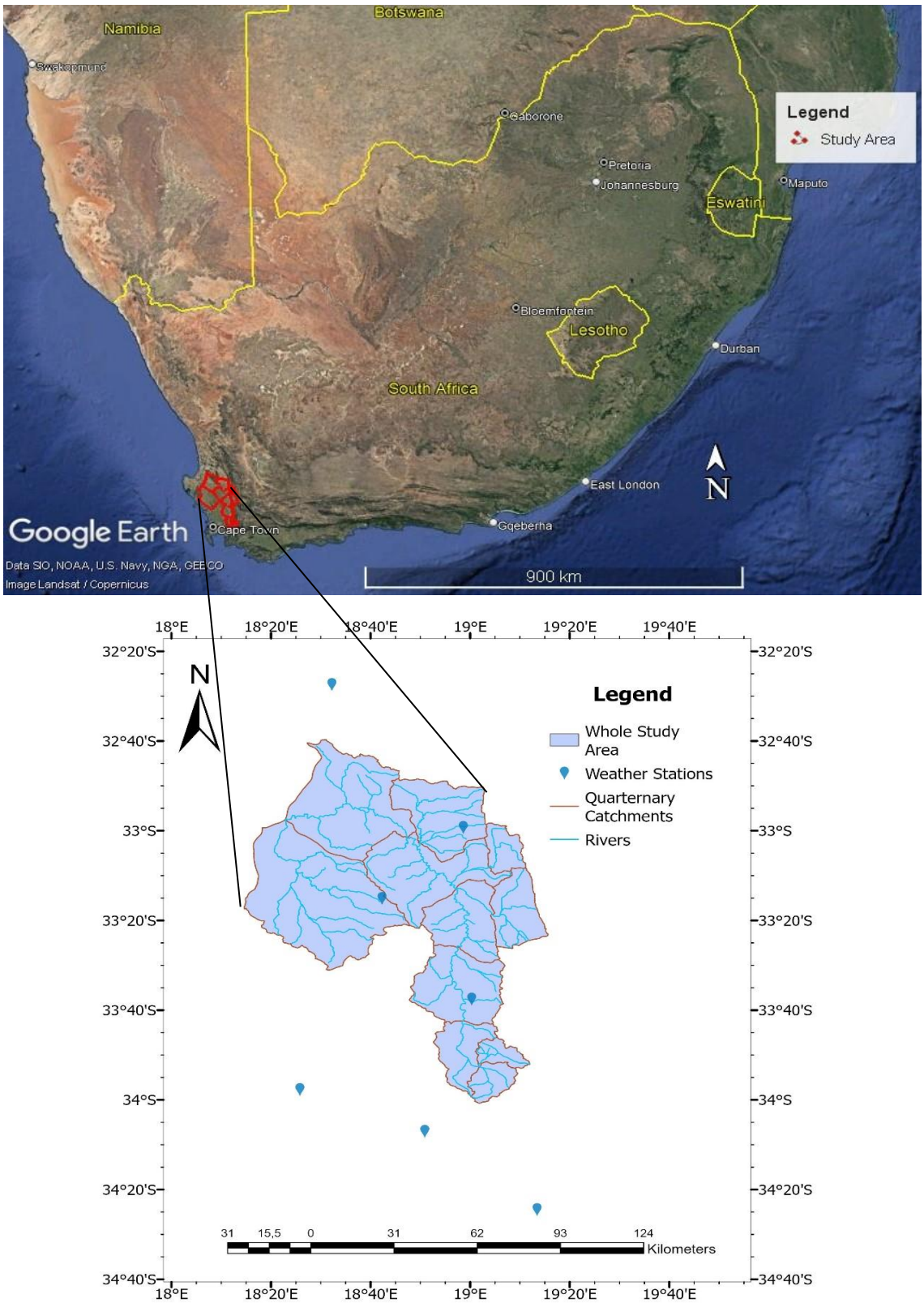

Figure 3.1: Location of the study area with a view of the quaternary catchment (source of image: Google Earth Pro 2024).

3.3 General Workflow

In Figure 3.2, the general workflow that was followed in this study can be seen in a summarized visual representation. Each step mentioned in the workflow was expanded on in the rest of this section.

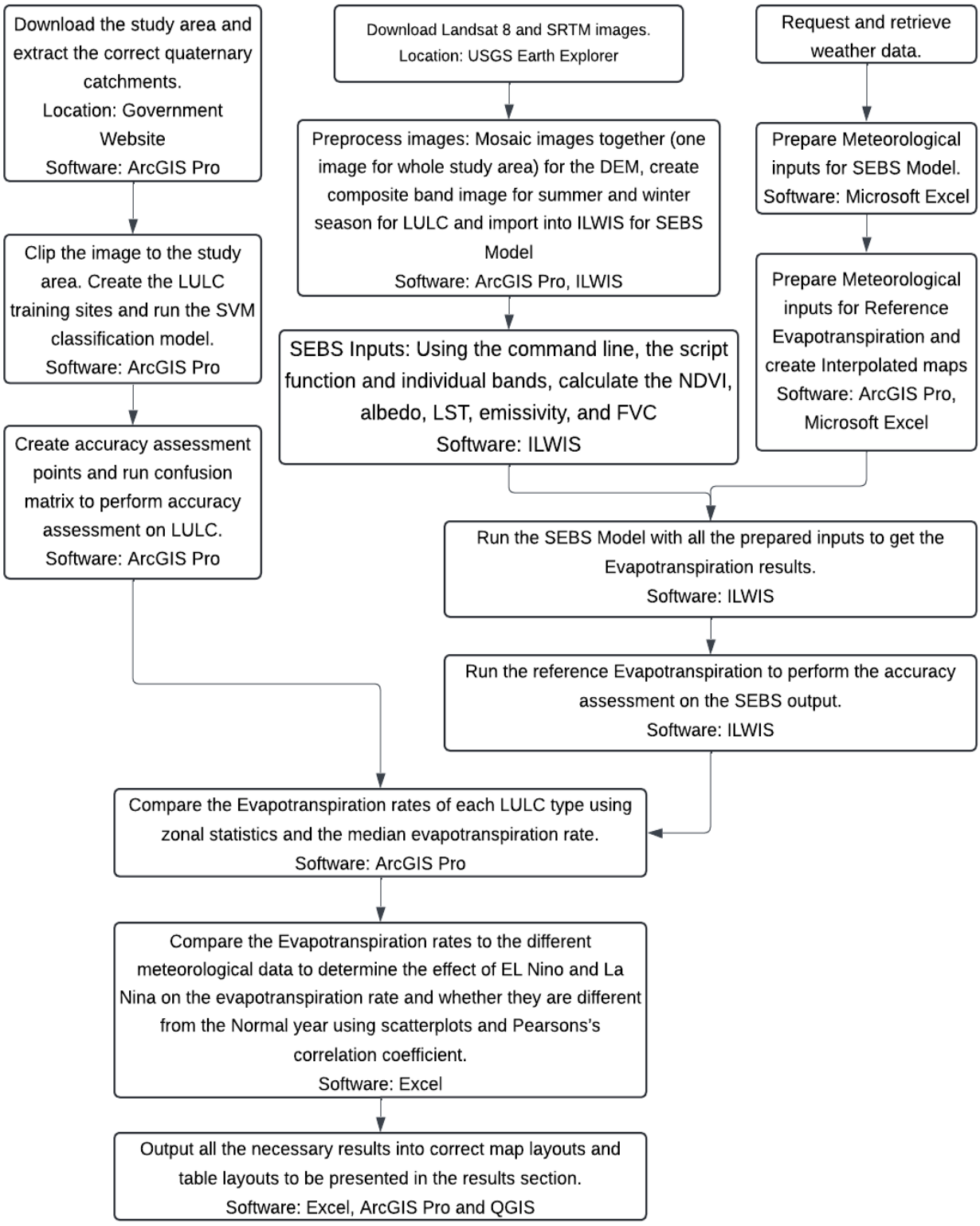

Figure 3.2: The general workflow that was followed to perform this study.

3.4 Satellite Imagery Preprocessing

Landsat 8 imagery was used for the LULC mapping for the SEBS model (Rwasoka *et al.*, 2011). Landsat 8 is a medium-resolution multispectral sensor that was launched in 2013. Table 3.1 provides the details of the specific band information for Landsat 8.

Table 3.1: Details of Landsat 8 bands

Band	Wavelength Range (micrometers)	Spatial Resolution (meters)	Description
1	0.43 - 0.45	30	Coastal/Aerosol
2	0.45 - 0.51	30	Blue
3	0.53 - 0.59	30	Green
4	0.64 - 0.67	30	Red
5	0.85 - 0.88	30	Near Infrared (NIR)
6	1.57 - 1.65	30	Shortwave Infrared 1 (SWIR-1)
7	2.11 - 2.29	30	Shortwave Infrared 2 (SWIR-2)
8	0.50 - 0.68	15	Panchromatic
9	1.36 - 1.38	30	Cirrus
10	10.60 - 11.19	100	Thermal Infrared 1 (TIRS-1)
11	11.50 - 12.51	100	Thermal Infrared 2 (TIRS-2)

The Landsat 8 Level 2 images with tile number 175083 were retrieved from the United States Geological Survey (USGS) EarthExplorer website (https://earthexplorer.usgs.gov/). Level 2 images were used as these images have already been atmospherically corrected. Details of the images are presented in Table 3.2.

Table 3.2: Details of the Landsat 8 images acquired and used in the study.

Season Used for	Date Captured
Summer 2015/6	09/01/2016
Autumn 2016	14/04/2016
Winter 2016	16/05/2016
Spring 2016	21/09/2016
Summer 2019/20	04/01/2020
Autumn 2020	21/02/2020
Winter 2020	11/05/2020
Spring 2020	08/09/2020
Summer 2020/1	05/12/2020
Autumn 2021	23/02/2021
Winter 2021	17/07/2021
Spring 2021	02/08/2021

One Landsat 8 image that covered the whole study area for each season (summer, autumn, winter, spring) for the years 2020/2021, 2019/2020, and 2015/2016 was downloaded for each season to be able to compare the different ET rates for different seasons within different Normal, La Nina and El Nino years. One image per season was used as most of the images in the Winter season experienced cloud cover, giving the freedom to find one image somewhere within the season with the least amount of cloud cover. The Landsat 8 images downloaded for summer and winter for each La Nina and El Nino year were also used to be able to determine the LULC for the different summer and winter seasons in the two different years.

The dates to search for images to find an image with minimal cloud cover for each season were set to be the 3 months of each season. The images that were chosen were chosen to be the closest date to the solstice or equinox covering the whole study area with as little cloud cover as possible. This was done for each season over the three years resulting in one image being downloaded for each season. The dates of each image that was downloaded can be seen in Table 3.2. The individual bands of each image downloaded were then imported into ILWIS 3.8.6 open-access software to be used for preparing the data for the SEBS Model.

Landsat 8 was chosen to estimate ET rates as it has proven to produce accurate results when used in combination with the ILWIS software SEBS model (Elkatoury *et al.,* 2020), it has good spatial coverage to cover the study area in one image without too low of a spatial resolution and its various bands record and produce all the required remote sensing information for the SEBS model. Landsat 8 was also chosen for the LULC cover analysis as it has a high spatial resolution which allows for a more detailed analysis of the different LULC types (Shoko *et al.,* 2015a; Pandey *et al.,* 2019; Elkatoury *et al.,* 2020) and or compatibility with derived ET estimates.

For the LULC assessment, the individual bands 1 to 7 were imported into ArcGIS to form one composite image for each summer and winter season for the La Nina and El Nino years. The bands were coastal/aerosol, blue, green, red, NIR, SWIR1 and SWIR-2. LULC on average does not change that much over the years on such a big scale, so the same LULC maps made for the 2020/2021 Summer and Winter seasons were used for the 2019/2020 year. The 4 images were then all clipped to the extent of the study area.

The SEBS model also needs a digital elevation model (DEM) as one of its inputs. The DEM was downloaded from USGS Earth Explorer using Shuttle Radar Topography Mission (SRTM) 1 Arc-Second Global data that collected the DEM at a 30m spatial resolution for the entire globe (https://gisgeography.com/free-global-dem-data-sources/). The spatial resolution is also compatible with the LULC and ET estimates. Four images were downloaded in Geotiff format to cover the whole study area. They were mosaiced together and clipped to fit the study area in ArcGIS Pro and imported into ILWIS to run the model.

3.5 Meteorological Data Inputs

Meteorological data was downloaded from 7 weather stations around the drainage basin area from: https://www.weathersa.co.za/home/aboutclimateatsaws. These weather stations are called: Cape Agulhas, Strand, Kirstenbosch, Wellington, Langgewens, Porterville, and Redelingshuys. They are all Automatic Weather Stations (AWS) which means they have the required data that is needed for the SEBS model. The required data includes daily temperature (°C), surface pressure (pa), wind speed (m/s), and humidity (kg/kg). Unfortunately, none of these stations had sunshine hours so the sunshine duration (hours) was downloaded from a central weather station called the Cape Town Weather Office. The weather stations that the data was acquired from do not record solar radiation. Therefore, it was calculated using the Allen *et al.* (1998) equation in ArcGIS Pro. All the inputs were prepared as required by the model in terms of unit conversions. For example, humidity was converted from percentage to kg/kg, and pressure was converted from hPa to Pa.

For the Reference ET the Ordinary Kriging interpolation method was used in ArcGIS Pro to create a map from the wind speed point data (Shoko *et al.*, 2015a). This method has been chosen as it has been proven to be the most accurate method to map meteorological data in various areas globally as well as in South Africa (Apaydin *et al.*, 2004; Coulibaly and Becker, 2007; Hofstra *et al.*, 2008). The specific variogram model used within the Kriging interpolation was chosen based on what model best fits the data for each interpolation, but mostly the spherical variogram model was used.

3.6 SEBS remote sensing inputs

The inputs required for the SEBS model include albedo (-), land surface temperature (K) (LST), emissivity (-), Fractional Vegetation Cover (FVC), and NDVI. These maps were derived from

the Landsat 8 satellite imagery that had been imported into the ILWIS software. The equations that were used for these various inputs are described in Table 3.3. These equations were inputted into the command line in ILWIS to create these various maps except for the NDVI which was created using the Script tool.

Table 3.3: The equations that were used to prepare SEBS remote sensing inputs

Inputs	Formula	Reference
NDVI Red band 4 and NIR band 5	NDVI = (NIR-R)/(NIR+R)	(Sobrino *et al.*, 2004)
FVC Using the statistics from the NDVI previously calculated	$FVC = \left(\frac{NDVI - NDVI_{min}}{NDVI_{max} - NDVI_{min}}\right)^2$	(Sobrino *et al.*, 2004)
Emissivity	$Emissivity = 0.004FVC + 0.986$	(Sobrino *et al.*, 2004)
Albedo Using bands 2,4,5,6 and 7	$\alpha = 0.356b_2 + 0.13b_4 + 0.373b_5 + 0.085b_6 + 0.072b_7 - 0.0018$	(Liang, 2000)
LST Using thermal bands 10 or 11 Some values retrieved from the metadata	(1) $RAD = M_L * Q_{cal} + A_L$, where M_L = RADIANCE_MULT_BAND_band number, Q_{cal} = corresponding band (band 10/11), A_L = RADIANCE_ADD_BAND_bandnumber. (2) $BT10 = \left(K2/(\ln(K1/L) + 1)\right)$ where, K1 = K1_CONSTANT_BAND_thermalbandnumber, K2 = K2_CONSTANT_BAND_thermalbandnumber, L = RAD (previously calculated). (3) $LST = [BT/(1 + (0.00115 * BT/1.4388) * \ln \varepsilon)]$ where BT = previously calculated for each band, Ln = natural log and ε = emissivity	(Fahdawi *et al.*, 2021)

Once all the input images were created, they were resampled using the nearest neighbor technique in ILWIS to ensure that they had the same geo-reference. Julian day was determined from the image acquisition date, the sun zenith angle was calculated from the Landsat 8 metadata and the reference height was calculated to be the average reference height of all the weather stations. This was also done for each season for the three years. Once the SEBS outputs were created for each season for the three years, the images were imported into QGIS to create the visual representation of the SEBS results that can be seen in the results section.

3.7 Land use land cover mapping from Landsat 8

Land use land cover maps are needed to understand their different ET for better water resource and land management planning. The SVM learning classification algorithm was used to classify the different land use and land cover types of the drainage basin. This classification method was chosen as it has been used successfully in previous similar studies and it is easier to define and requires fewer user-defined parameters in comparison to other classification methods (Shoko *et al.,* 2015a; Pandey *et al.,* 2019; Nasiri *et al.,* 2022). First, the composite Landsat 8 image was loaded into ArcGIS Pro. The LULC classes chosen for the analysis are water, shrub, grassland, agriculture, bare land, and built-up area. The training sites for these LULC types were then created using the Landsat 8 image in ArcGIS Pro software and the create training samples tool with a Google Earth map linked for reference. The SVM learning algorithm was then run to classify the different LULC classes in the study area. This was done once for each summer and winter season for the two respective years, 2015/2016 and 2020/2021.

3.8 Accuracy assessment

3.8.1 SEBS model accuracy

The ET estimates derived from SEBS were compared to ground-based results both of which are actual ET rates as estimated using the different techniques for the study area. For the ground-based results, the estimated ET rates were calculated using the equations from Allen *et al.* (1998) which is a widely accepted method for accuracy checking of this model. This is known as reference evaporation and is used to validate remote sensing-based estimates (Rwasoka *et al.,* 2011; Shoko *et al.,* 2015a). This was also done in the ILWIS software using only the wind speed interpolated weather maps, the DEM, the average daily relative humidity, maximum daily temperature, minimum daily temperature, average daily temperature, solar net radiation at crop surface, and the Julian day number.

To perform the validation, 50 random points were created in ArcGIS excluding the 3 weather stations within the study area, the SEBS ET and the reference ET maps were imported into ArcGIS, and then the ET value was extracted and added to the attribute table of the 50 points for each season in the three years. The points were divided into distances from the weather station in 15km intervals from 0 to 60km to see if the distance from the weather station affects the accuracy of the estimations. These attribute tables were exported into Excel and the average

difference for each distance category was calculated for each season. This was done for each season for the three years. Then the average difference for each distance category was calculated. The RMSE was also calculated to determine the accuracy of the SEBS ET and Reference ET using the SEBS ET and reference ET of the 50 points and calculating the RMSE in Excel. Visually, the reference ET and the SEBS ET maps were also compared to see if the overall spatial pattern of ET was the same.

3.8.2 LULC classification accuracy

The accuracy of the image classification for the different LULC classes was also assessed, using the confusion matrix method in ArcGIS Pro. This method was chosen as it is one of the most common methods used when performing accuracy assessments on LULC classifications (Chughtai *et al.*, 2021). Firstly, 100 points for each different LULC type were collected into a point layer in ArcGIS Pro using the satellite image and a linked Google Earth image. Using the confusion matrix tool, the confusion matrix was calculated from the classified and ground truth values for each point to determine the producer, user, and overall accuracy as well as the kappa statistics of the classification. This was done for each classification in each season for the two years.

3.9 Comparison of ET

3.9.1 Comparison of ET estimates among different LULC types

To compare the ET per LULC type in the study area, zonal statistics and zonal statistics to table tools were used within ArcGIS Pro to calculate the median ET rate of each LULC type and output the results as a table and as a map. This was done for each summer and winter season in the three years and then the tables were compared to see if the different LULC types affected the ET rates.

3.9.2 Comparison of ET estimates between El Nino, La Nina, and the normal year

Using the averages experienced each day of each season of the meteorological data and the daily ET rate that is experienced in each season created by the SEBS Model, a comparison was done to determine if a relationship exists between the El Nino and La Nina events and the ET rates and if they are different from the Normal year ET rates. This was done in Excel by creating scatterplots to determine visually if a relationship exists between ET rates and different meteorological parameters and where the relationship is strongest. The Pearson correlation was

also calculated to determine the strongest relationship between the average daily meteorological data experience for the study period and the average daily ET rates experienced for the study period and whether the different El Nino and La Nina events affected the relationships and were different from the Normal year.

3.10 Summary of the Chapter

This chapter focused on the methods used in this study to achieve the aim and objectives of the study. The study site was expanded on and the workflow was illustrated and then expanded on in detail in the sections that followed. The chapter explained how the satellite images were downloaded and preprocessed, the meteorological data was retrieved and prepared, the SEBS inputs were prepared, the LULC classifications were performed, the SEBS model was run, and the accuracy assessments were performed. The last section of the chapter explained how the comparisons between the ET and climatic events and ET and LULC types were performed. The results from the methodology explained in this chapter are presented in the next chapter.

CHAPTER FOUR: RESULTS

4.1 Introduction

This section highlights the results of the research done to achieve the aim of determining the ET rates of different LULC classes and the effects of climatic phenomena on ET. The SEBS model was run to determine the ET rates within the study area for each season for the two different climate events (El Nino and La Nina years) in 2015-2016 and 2020-2021 and for the Normal year, 2019-2020 to see if the climatic events affect the ET rates. The SVM classification was performed to determine the LULC of the study area for the 2015/2016 and 2020/2021 years. Using the LULC classifications a comparison was made of the ET and the different LULC classes to determine what the effect of the different classes are on the ET rate. The figures and tables created to achieve all the objectives are presented in this section and described in detail.

4.2 Seasonal variation in SEBS-derived ET estimations during the different climatic events

Generally, ET between the seasons varies significantly, and this is why the same range of values in the symbology could not be used for the different seasons. The maps with the same legend are presented in Appendix two. These maps show the variations in ET across the different seasons for the different climatic events and the normal year. However, they mask the variations in ET across the study site. The image acquired in the summer seasons had the highest average ET rates (3.47mm/day on average for all the years) and the winter season had the lowest ET rates (0.96mm/day on average for all the years). The image acquired in the autumn season had a higher average ET (2.59mm/day on average for all the years) than the spring season (1.48mm/day on average for all the years). In all the seasons of all the years, one can see that the waterbody (on the eastern side of all the maps) is an area of low ET (Figures 4.1-4.4). The general spatial pattern of the ET throughout the study area is similar with similar areas having low and high values in all images and more the rate of ET changing rather than the location.

When comparing the different seasons of the El Nino and La Nina years, one can see that in general, the La Nina seasons have a greater ET of 2.39mm/day ET average for the year than the El Nino seasons which has a 2.36mm/day average ET for the year. When comparing the

climatic events to the normal year, on average, all the seasons have a higher ET rate than the normal year for both climatic events as the normal year's average daily ET is 1.62mm.

Figure 4.1 illustrates the spatial pattern of ET across the study area for all three acquired images in the summer seasons over the three years. The image acquired in the summer season has more areas covered with higher ET rates than any other season. The La Nina summer season (2020-2021) (Figure 4.1c) also has a higher maximum ET rate of 7.253mm/day as opposed to 4.806mm/day of the El Nino year (2015-2016) (Figure 4.1a) and a higher average ET of 4.338mm/day as opposed to 3.563mm/day. The maximum ET rate for the summer season in the normal year (2019-2020) (Figure 4.1b) is lower than both years at 4.293mm/day and the average ET rate is also lower than both climatic events at 2.499mm/day. The lower ET rates in general can be seen on the eastern side of the study area in all three years with the western side showing higher ET rates. The middle of the study area shows slightly lower ET rates than the western side for the climatic event years with these lower values being further north in the 2015-16 summer as opposed to the 2020-21 summer. The middle section of the normal year shows different characteristics to the climatic events with the ET rates just alternating between higher and lower values.

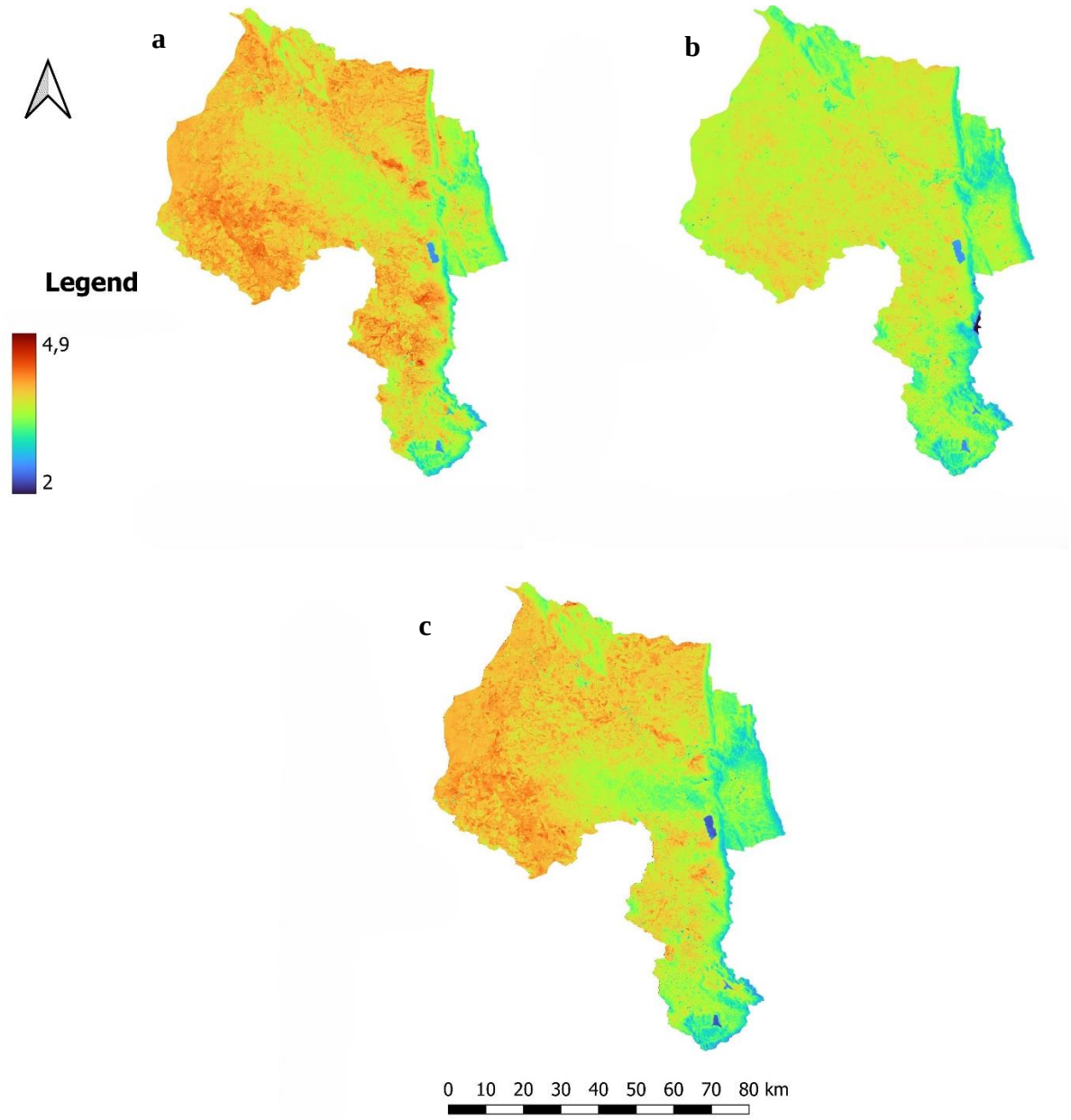

Figure 4.1: SEBS derived ET rates for the summer seasons in the El Nino (2015-16) (a), normal (2019-20) (b) and La Nina (2020-21) (c) year

Figure 4.2 illustrates the ET rates for the autumn seasons in each of the different climatic event years. The El Nino year is Figure 4.2a, the normal year is Figure 4.2b and the La Nina year is Figure 4.2c. The images acquired for the autumn seasons have a much higher ET rate in 2021 (La Nina) as opposed to 2016 (El Nino). The normal year has an even higher ET rate across the study area than the La Nina year. In general, the spread of the ET rates can be seen to be lower on the eastern side of the study area and higher on the western side of the study area. Once again, there are two areas of low ET which are sections in the middle eastern and southern

parts of the study area. The average daily ET rate of the autumn season for the study area in the La Nina year is 2.728mm, with a maximum of 5.845mm and a minimum of 0mm, the average daily ET rate of the autumn season for the study area for the El Nino year is 2.411mm with a maximum of 4.036mm and a minimum of 0.925mm and the average daily ET of the autumn season for the study area for the Normal year is 2.636mm with a maximum of 3.387mm and a minimum of 1.767mm. This shows that the maximum and average ET rate of the La Nina year is higher in the autumn month and the minimum of the La Nina year is lower in the autumn month than the El Nino year. The normal year has a higher average ET rate than the El Nino year but lower than the La Nina year. The maximum values of both climatic events are higher than the normal year and the minimum values of both climatic events are lower than the normal year.

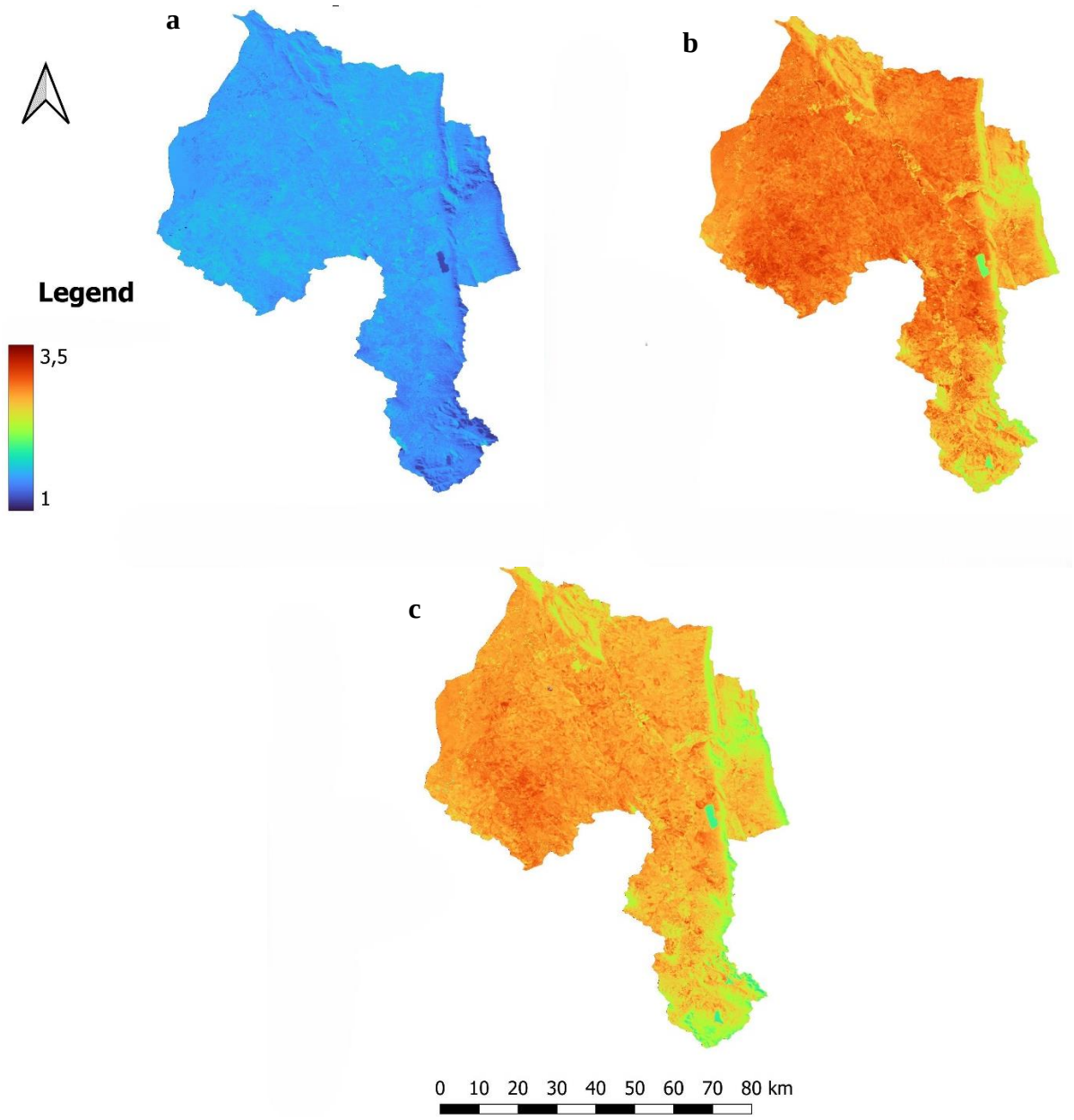

Figure 4.2: SEBS derived ET rates for the autumn seasons in the El Nino (2015-16) (a)), normal (2019-20) (b)), and La Nina (2020-21) (c)) years.

Figure 4.3 shows the SEBS-derived ET rates for the winter seasons for the El Nino year (Figure 4.3a), normal year (Figure 4.3b), and La Nina year (Figure 4.3c). The satellite image for the winter season of 2016 contained cloud cover in the southern section of the study area skewing the ET results in this part of the study area slightly for this season. Figure 4.3 shows that the northern part of the study area in the El Nino winter season (2015-2016) (Figure 4.3a) seems to in general have a higher ET rate than this area in the La Nina winter season (2020-2021) (Figure 4.3c). However, the southern area in the El Nino year has a much lower ET rate than

the southern area of the La Nina winter season. The normal year (2019-2020) (Figure 4.3b) however, over the whole study area seems to have much higher ET rates than any of the other two years. In general, for the wither seasons, except for the southern section of the study area, the general spatial distribution of the ET rate in all three years for the winter season is quite similar with less variation across the study area than seen in other seasons. Referring to the average, minimum, and maximum values of ET, the El Nino year for the winter season has a lower minimum (0.061mm/day), maximum (1.915mm/day), and average (0.878mm/day) value than the La Nina minimum (0.27mm/day), maximum (2.225mm/day) and average (1.215mm/day) value. The normal year's ET minimum value (0.425mm/day) is higher, the maximum value (1.054mm/day) is lower and the average value (0.781mm/day) is lower than both climatic events.

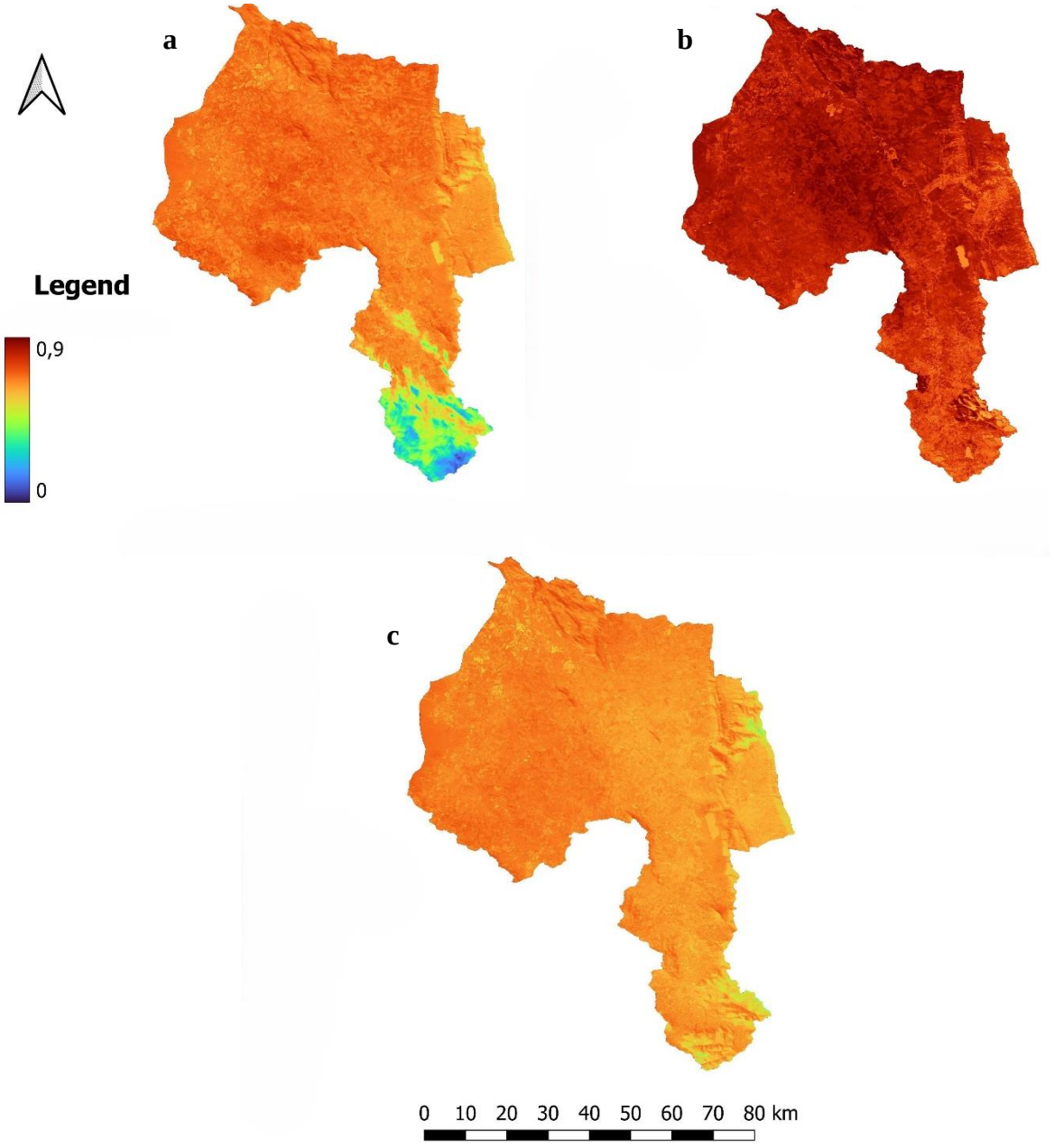

Figure 4.3: SEBS derived ET rates for the winter seasons in the El Nino (2015-16) (a)), normal (2019-20) (b)), and La Nina (2020-21) (c)) years.

Figure 4.4 illustrates the SEBS-derived ET values for the spring season for the three years with Figure 4.4a being the El Nino year, Figure 4.4b being the normal year and Figure 4.4c the La Nina year. These images for the spring season (Figure 4.4) show the most variation in values throughout the three years when compared to the other seasons with the El Nino season (Figure 4.4a) having in general a much higher ET rate across the study area than the La Nina season (Figure 4.4c) and the normal year (Figure 4.4b) being much lower than both climatic events for this season. The minimum, maximum, and average ET rates of this season's results reflect

the same idea as what is shown in Figure 4.4 with the minimum (0.84mm/day), maximum (4.832mm/day) and average (2.583mm/day) values of the El Nino spring season being higher than the minimum (0.311mm/day), maximum (2.38mm/day) and average (1.284mm/day) values of the La Nina spring season and the minimum (0.269mm/day), maximum (0.938mm/day) and average (0.938mm/day) values of the normal year being much lower than the El Nino and La Nina years.

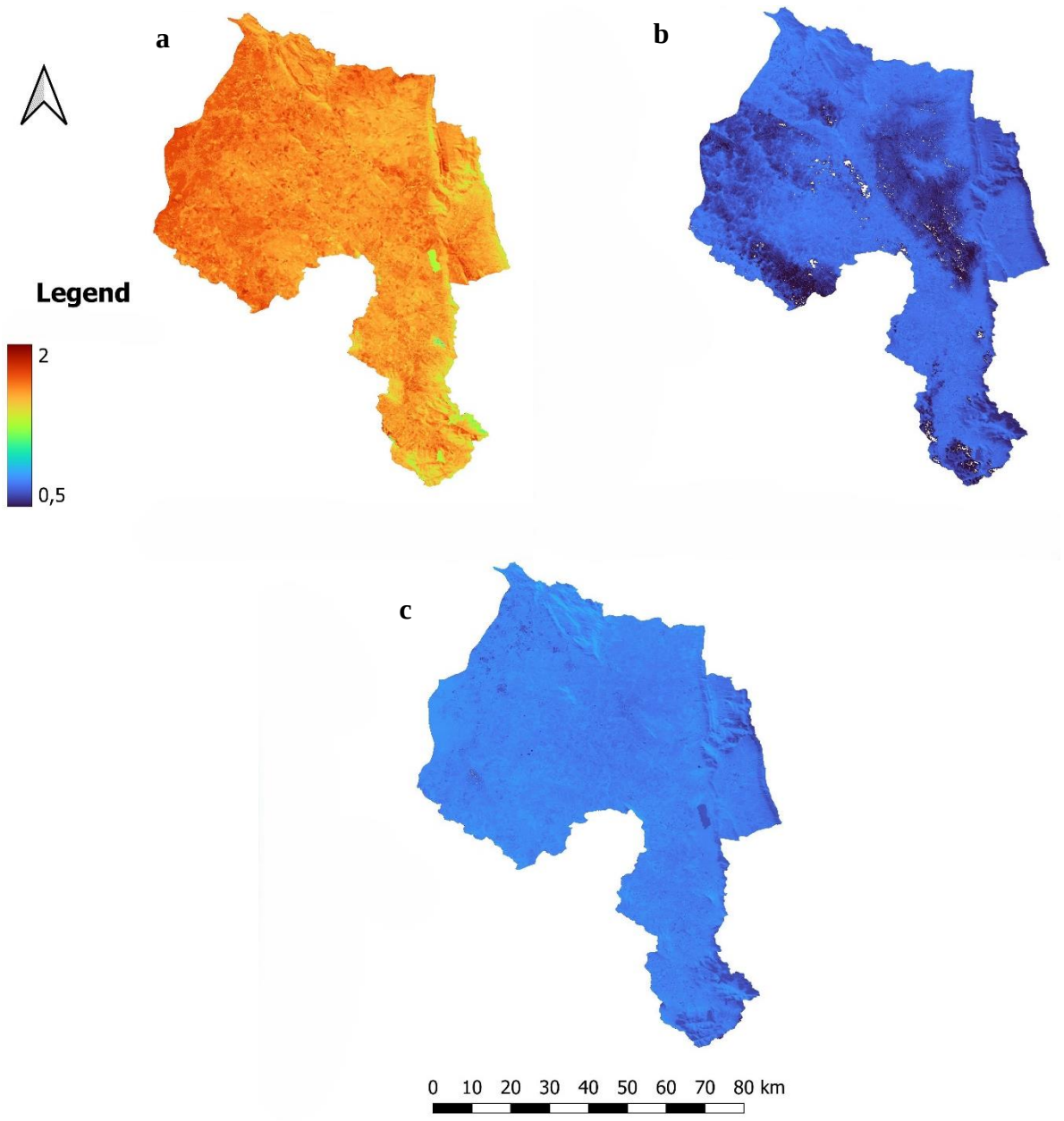

Figure 4.4: SEBS derived ET rates for the spring seasons in the El Nino (2015-16) (a)), normal (2019-20) (b)), and La Nina (2020-21) (c)) years.

4.2.1 Assessment of SEBS-derived ET estimations accuracy

The results of the reference ET can be seen in Figures 4.5, 4.6, and 4.7. Figure 4.5 shows the summer (a), autumn (b), winter (c), and spring (d) ET rates for the El Nino year (2015-2016). Figure 4.6a, b, c, and d show the summer, autumn, winter, and spring seasons, respectively, for the normal year (2019-2020). Figure 4.7 illustrates the different seasons for the La Nina year, summer (a), autumn (b), winter (c), and spring (d). When calculating the reference ET an interpolated wind map is used. The maps in the figures show the effects of the interpolated wind map on the estimating of the ET rate using only ground truth data for the whole study area. The two main dots in all the maps are where two of the three weather stations are situated (in the center of the study area and the northeastern part of the study area) showing the effects of the collection points on estimating the areas away from the collection points. These figures also illustrate that as with the SEBS ET, the summer season has the highest ET, the winter season has the lowest ET, and the autumn season has a higher ET than the spring season.

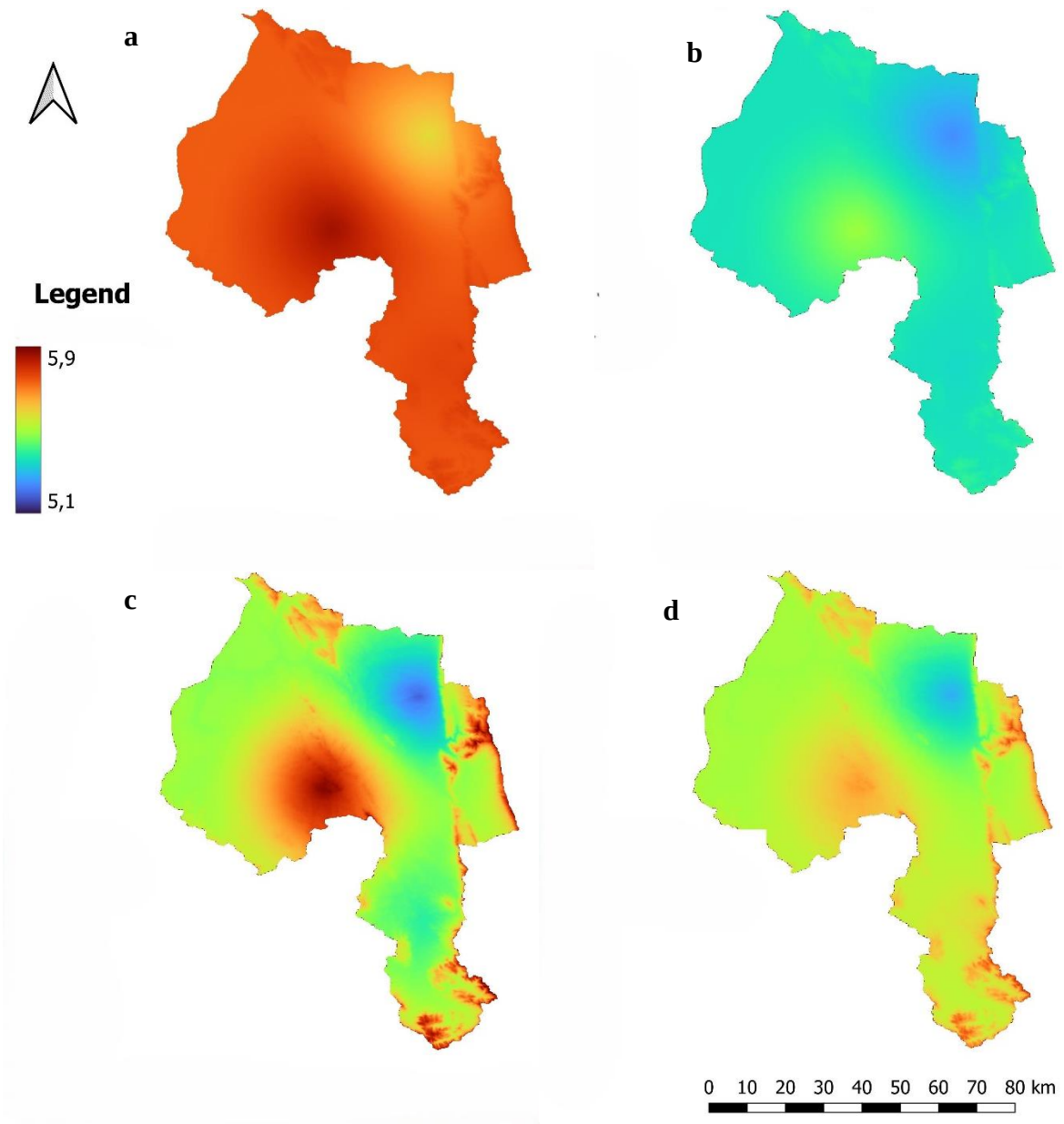

Figure 4.5: Seasonal Reference ET rates in the El Nino year 2015-2016 representing: (a) Summer 2015-2016, (b) Autumn 2016, (c) Winter 2016, (d) Spring 2016.

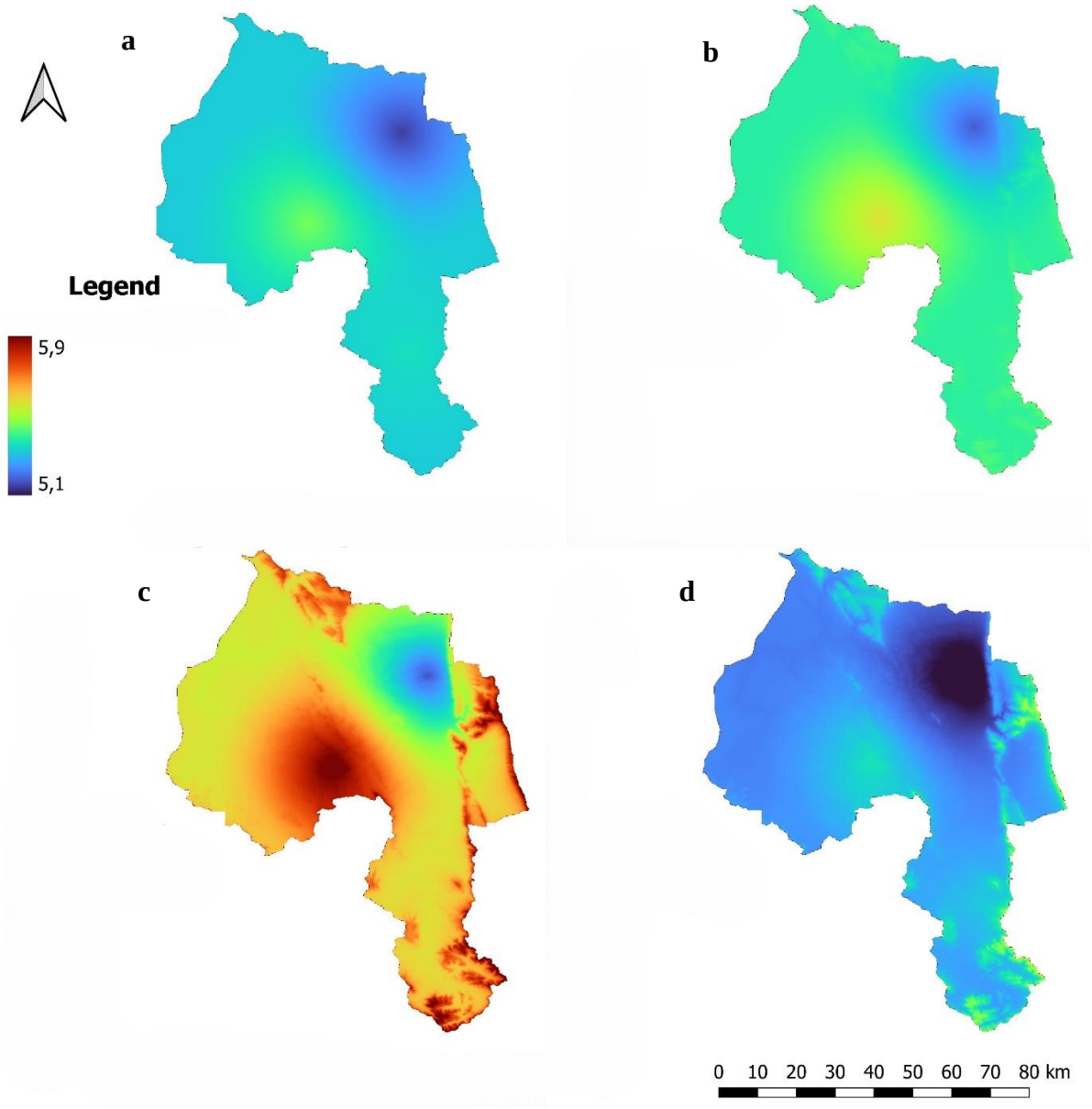

Figure 4.6: Seasonal Reference ET rates in the Normal year 2019-2020 representing: (a) Summer 2019-2020, (b) Autumn 2020, (c) Winter 2020, (d) Spring 2020.

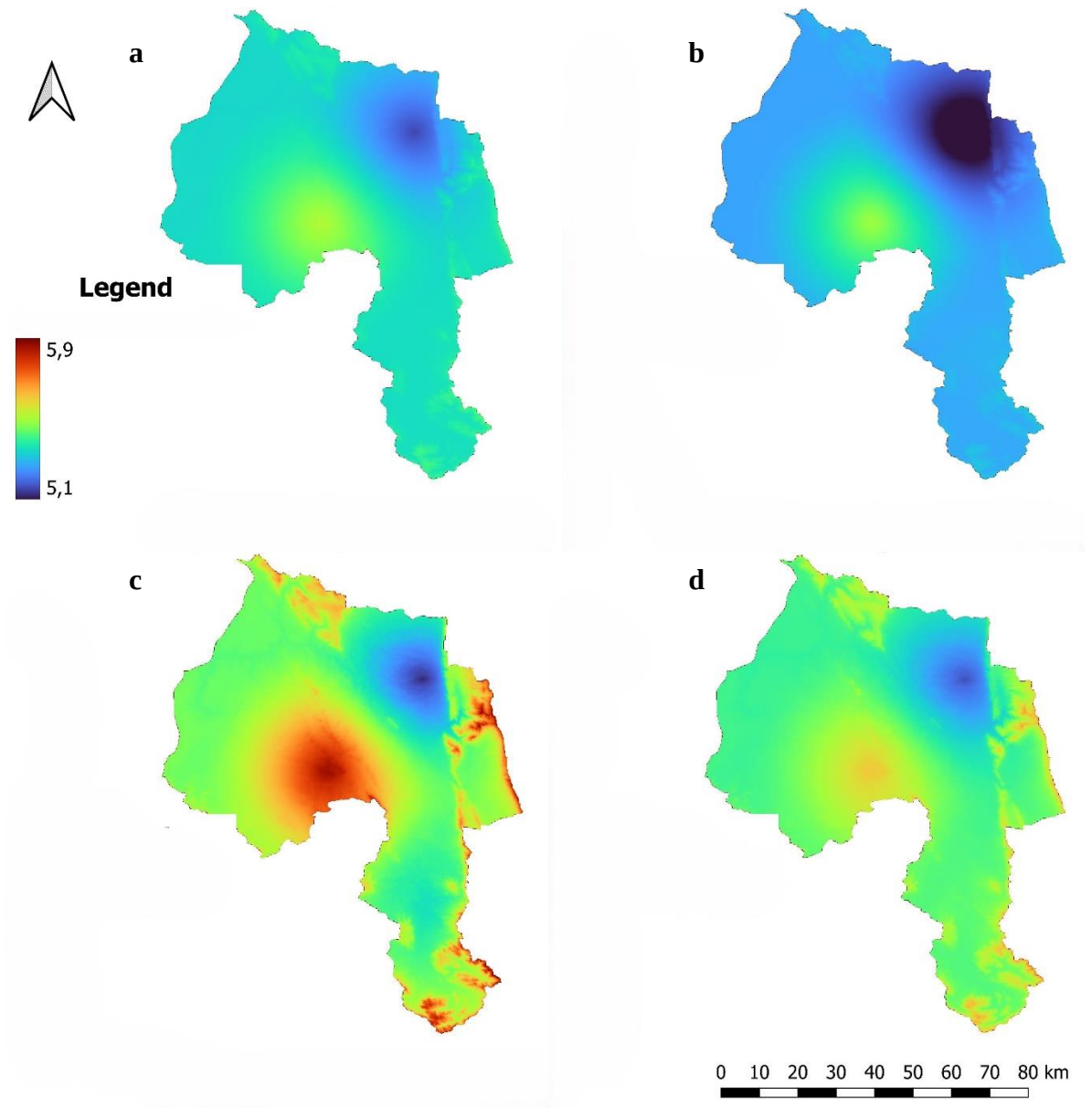

Figure 4.7: Seasonal Reference ET rates in the La Nina year 2020-2021 representing: (a) Summer 2020-2021, (b) Autumn 2021, (c) Winter 2021, (d) Spring 2021.

Comparing each SEBS-based ET estimate to the reference ET map for each season for the three years shows visually that the general spatial pattern of the change in the ET rates across the study area is the same, especially on the eastern side of the map where the elevation of the study area is affecting the ET rate. Visually, the SEBS model predicts a similar ET distribution pattern across the study to the reference ET.

The exact minimum, maximum, and average values of the reference ET and the SEBS model ET are shown in Table 4.1. When comparing these values, and not looking at the visual spread

of the data, one would think that the accuracy of the model is very poor due to the big difference between the reference value and the SEBS model value. However, the wind speed data had to be interpolated so, the accuracy of the reference ET data is not necessarily accurate across the whole study area. To determine if the distance from the weather station affects the similarity of the ET rates, the average difference between the SEBS ET and reference ET for all seasons was calculated at the different distance intervals from the weather stations and these results are shown in Table 4.2.

Table 4.1: The temporal statistics of SEBS-derived and the reference ET.

Season	Statistic Parameter	SEBS Eto	Reference Eto
Su2015-16	**Min**	2.319	5.5789
	Max	4.806	5.8625
	Average	3.563	5.7208
Au2016	**Min**	0.925	4.1781
	Max	4.036	8.2114
	Average	2.411	4.3364
Wi2016	**Min**	0.061	2.8223
	Max	1.915	4.3707
	Average	0.878	2.9179
Sp2016	**Min**	0.84	3.3909
	Max	4.832	5.3613
	Average	2.583	3.5202
Su2020-21	**Min**	2.184	5.1582
	Max	7.253	9.7257
	Average	4.338	5.3389
Au2021	**Min**	0	3.8776
	Max	5.845	8.9384
	Average	2.728	4.1865
Wi2021	**Min**	0.27	2.8062
	Max	2.225	4.3139
	Average	1.215	2.9055
Sp2021	**Min**	0.311	3.3354
	Max	2.38	5.0959
	Average	1.284	3.4678
Su2019-20	**Min**	0.505	5.1492
	Max	4.293	9.7004
	Average	2.499	5.3087
Au2020	**Min**	1.767	4.1042
	Max	3.387	8.9841
	Average	2.636	4.3494
Wi2020	**Min**	0.425	2.8175
	Max	1.054	4.4022
	Average	0.781	2.9267
Sp2020	**Min**	0.269	3.2636
	Max	0.938	4.8926
	Average	0.561	3.3944

Table 4.2 shows the results of the RMSE of the SEBS-derived ET in comparison to the Reference ET. The RMSE for the summer season is the lowest with an average of 33%, followed by 46% for the autumn season, 72% for the spring season, and the highest RMSE in the winter season with an average of 76%. The overall RMSE for the study period for all the seasons is 57%.

Table 4.2: The RMSE for the different seasons in the different climatic event years between the SEBS ET and Reference ET.

Season	**RMSE (%)**
2015-16 Summer	34.5250
2016 Autumn	64.9845
2016 Winter	77.7548
2016 Spring	54.9753
2019-20 Summer	34.0278
2020 Autumn	35.8960
2020 Winter	72.3758
2020 Spring	80.7757
2020-21 Summer	31.3316
2021 Autumn	36.6937
2021 Winter	77.4526
2021 Spring	78.7767
Average RMSE for the study period	**56.6308**

The results in Table 4.3 show that the average differences between the SEBS ET and the reference ET for the different distances from the weather stations are very similar with only a 0.08 maximum difference between the averages. This shows that across the study area, regardless of the distance from the weather stations, the distribution of the ET rates is roughly the same for both the SEBS ET and the reference ET. This agrees with what is shown visually, meaning that it is shown once again that the SEBS output is accurate enough to be used for the analysis in the rest of this study.

Table 4.3: The average differences between the SEBS-derived and reference ET rates at increasing distances from the weather stations.

Differences between SEBS Eto and Reference Eto					
Distance From the weather station	**At Weather Station**	**Within 15km**	**Within 30km**	**Within 45km**	**Within 60km**
2015-16 Summer	1.7768	1.9197	1.9415	2.1011	1.8982
2016 Autumn	2.7778	2.8200	2.8087	2.8356	2.8153
2016 Winter	2.2104	2.2341	2.2665	2.2948	2.2267
2016 Spring	1.9169	1.9247	1.9470	1.9522	1.8488
2019-20 Summer	1.7719	1.7787	1.7824	1.8648	1.7607
2020 Autumn	1.5893	1.5391	1.5612	1.5938	1.5034
2020 Winter	2.1041	2.1041	2.1322	2.1273	2.0850
2020 Spring	2.7497	2.7462	2.7270	2.7409	2.6712
2020-21 Summer	1.6602	1.6875	1.6042	1.7510	1.5342
2021 Autumn	1.5353	1.5250	1.5158	1.5899	1.5355
2021 Winter	2.2266	2.2416	2.2430	2.2590	2.2411
2021 Spring	2.7012	2.7197	2.7289	2.7481	2.7331
Average of Differences	**2.0850**	**2.1034**	**2.1049**	**2.1549**	**2.0711**

4.2.2 Trends in meteorological variations between different climatic events

Figures 4.8 to 4.12 visually represent the differences in meteorological data between the different seasons of different climatic events and the normal year. These values were derived from the average of the daily measurements for each season. In general, there is seasonal variation in all the meteorological parameters. However, the variation between the different climatic events themselves and the variation between the normal year and the climatic events is less distinct. For humidity (Figure 4.8), the summer and autumn seasons are slightly higher in the El Nino year (55.69% and 64.17% respectively) than the La Nina year (59.47% and 63.79% respectively), but the winter and spring seasons are slightly lower in the El Nino year 72.12% and 68.73% respectively compared to 72.69% and 69.23%). The normal year is lower

than both climatic events in the summer (59.45%) and autumn (63.08%) seasons but higher than both climatic events in the winter (73.62%) and spring seasons (70.49%).

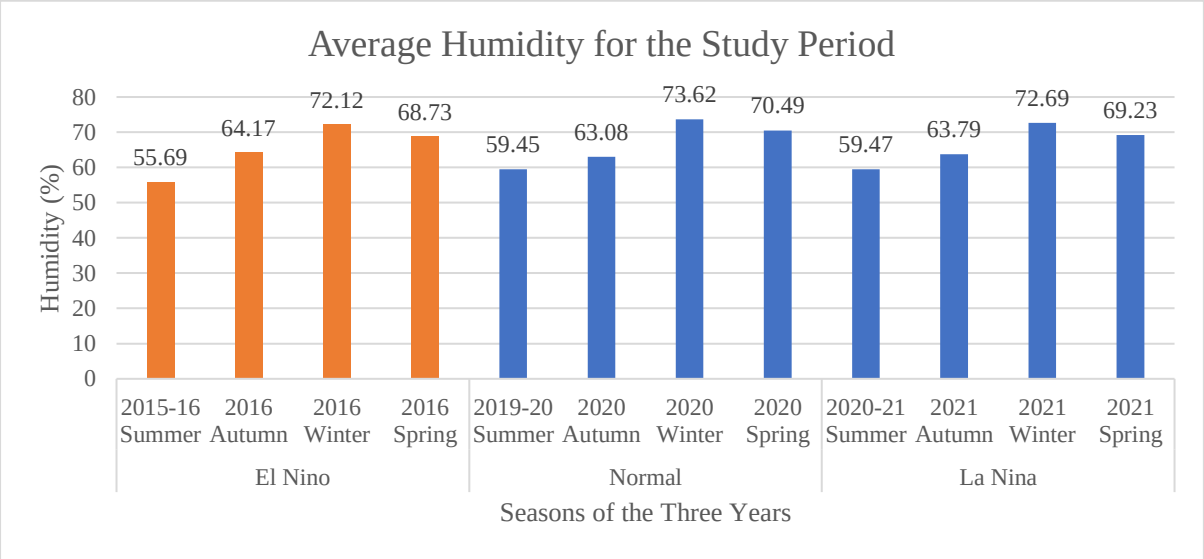

Figure 4.8: Seasonal humidity for the El Nino in 2016, Normal year in 2020, and La Nina in 2021.

The wind speed (Figure 4.9) shows slightly higher values in the autumn (0.07m/s higher) and winter (0.03m/s higher) seasons in the El Nino year and slightly lower average wind speed in the summer (0.06m/s lower) and spring (0.15m/s lower) seasons when compared to the La Nina year. The normal year has a lower average wind speed in the summer (0.08m/s average lower), autumn (0.11 m/s average lower), and winter (0.16m/s average lower) seasons than both climatic events and a higher average wind speed in the spring season than the El Nino (0.15m/s lower) event but the same average wind speed in the spring season for the La Nina climatic event.

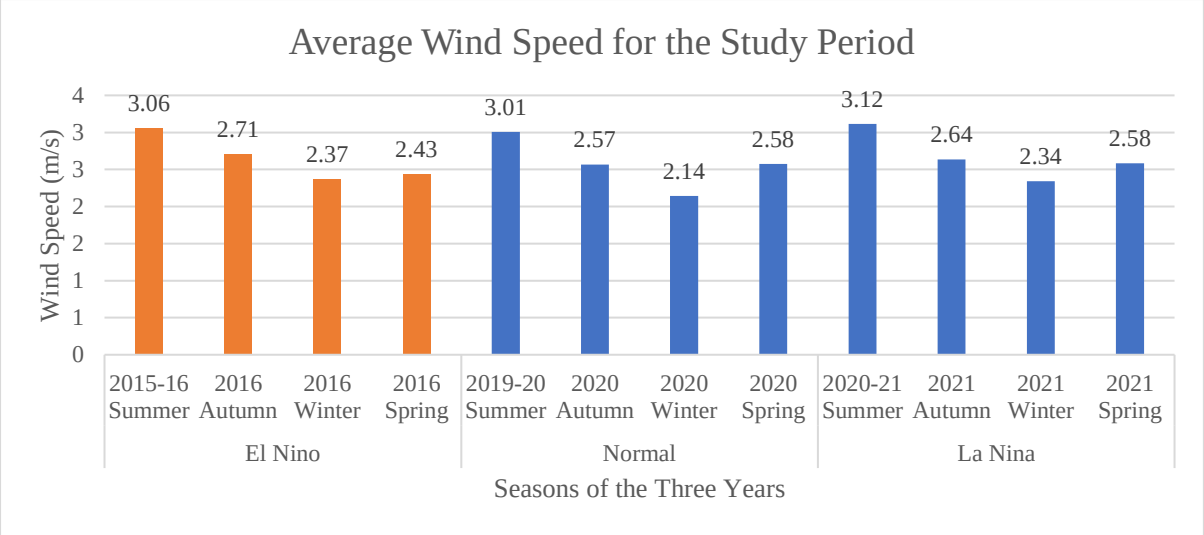

Figure 4.9: Seasonal wind speed for the El Nino in 2016, Normal year in 2020, and La Nina in 2021.

The biggest difference between the climate events within the meteorological data is in the surface pressure (Figure 4.10) between the winter seasons where the El Nino and normal year winter seasons have a much higher average pressure than the La Nina winter season with the El Nino winter season being the highest out of the three winter seasons. The surface pressure for all the seasons is at an average of 4.265hPa higher in the El Nino year than in the La Nina year. However, for the normal year, in the summer and winter seasons, it is lower (1.4hPa and 0.91hPa respectively) than the El Nino year but higher than the La Nina year (0.41hPa and 12.91 respectively), in the autumn season it is higher than both climatic events (average of 0.31hPa higher), and in the spring season, it is lower than both climatic events (average of 1.57hPa lower).

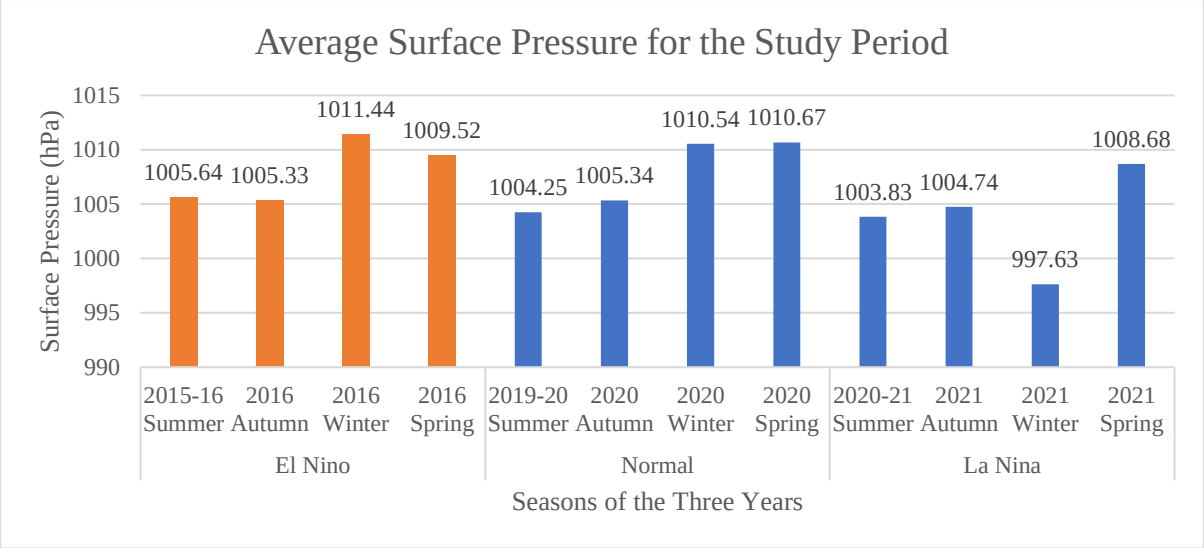

Figure 4.10: Seasonal surface pressure for El Nino in 2016, Normal year in 2020, and La Nina in 2021.

Figure 4.11 shows a comparison graph of the mean daily temperature for the different seasons for the different years in the study period. There was a relatively significant difference in temperature in the autumn season as illustrated where the El Nino and normal year temperatures are respectively 6.35°C and 7.22°C higher than the La Nina autumn temperature with the normal year being the highest in this season for the three years. The temperature in the summer and spring seasons in the El Nino year is also higher by 1.1°C and 0.72°C respectively than in the La Nina year but the winter season has a slightly lower average by 0.08°C than the La Nina year. The normal year has an average temperature that in the autumn and winter is higher by an average of 4.05°C and 0.82°C respectively than both climatic events but, in the summer and spring, is lower by an average of 0.59°C and 0.44°C respectively than both climatic events.

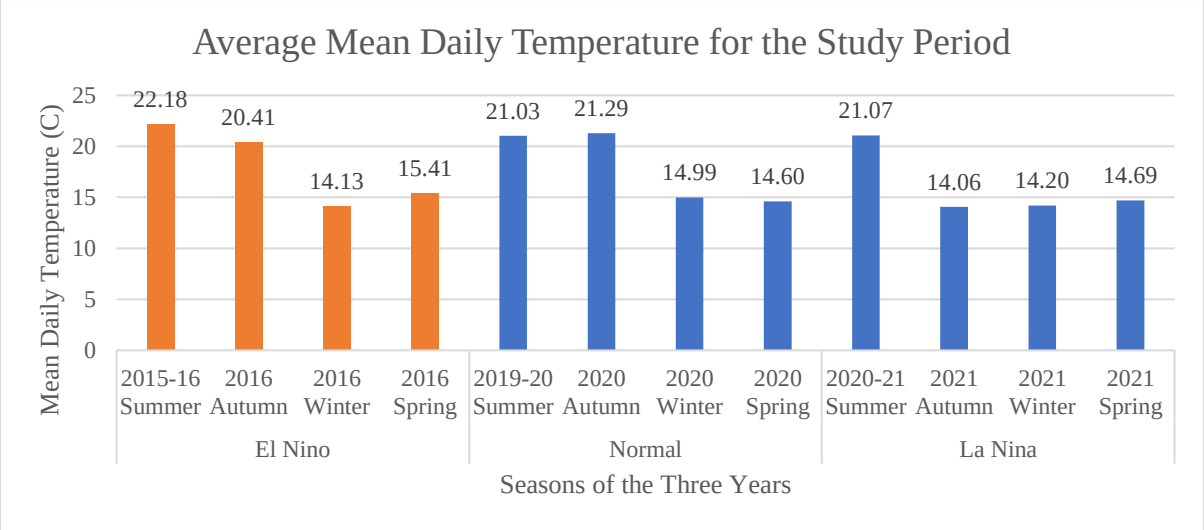

Figure 4.11: Seasonal mean daily temperature for the El Nino in 2016, Normal year in 2020, and La Nina in 2021.

The sunshine hours (Figure 4.12) are higher in the summer and winter seasons for the El Nino year by 0.87 and 0.02 hours respectively and lower in the autumn and spring seasons by 0.07 and 0.9 hours respectively when compared to the La Nina year. When compared to the normal year, the normal year is higher than both climatic events in the winter by an average of 0.56 hours, the same as the La Nina year but lower than the El Nino year by 0.87 hours in the summer, and higher than the El Nino year by 0.03 hours and 0.33 hours respectively but lower than the La Nina year by 0.03 hours and 0.57 hours respectively in the autumn and spring.

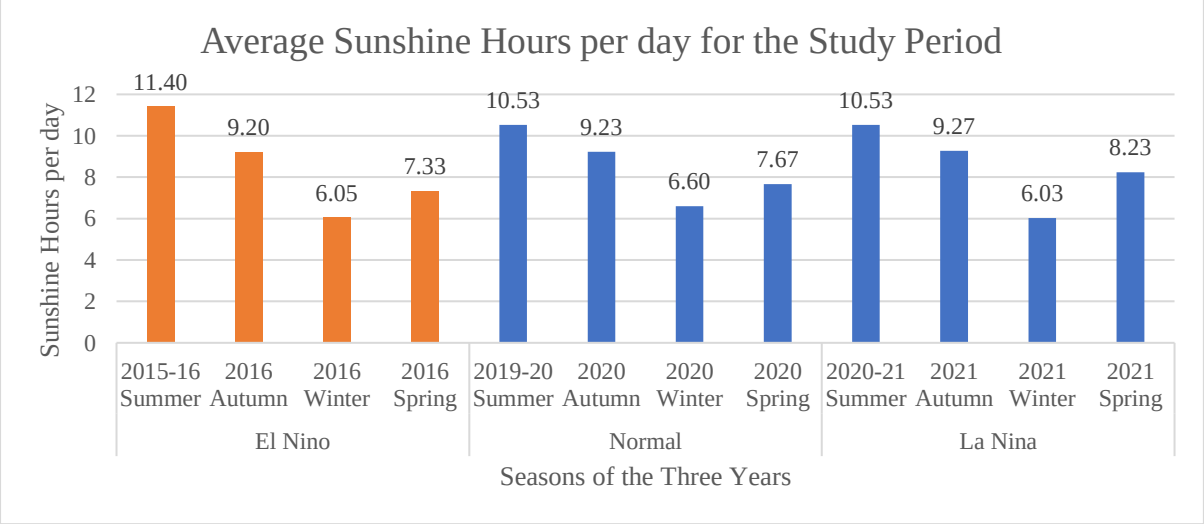

Figure 4.12: Seasonal sunshine hours for El Nino in 2016, Normal year in 2020, and La Nina in 2021.

4.2.3 SEBS-derived ET variations in relation to climatic events

Figures 4.13 to 4.16 visually represent the comparison between the ET rate and the different meteorological data parameters. Visually, in Figures 4.13 to 4.16, it is shown that the ET rate is highest in the La Nina year, followed by the El Nino year, and then lowest in the normal year. Figure 4.13 shows the visual comparison between ET and mean daily temperature for all three climatic events. The temperature for the La Nina year is higher than the El Nino year with the normal year having the lowest temperatures in comparison to the El Nino and La Nina years. A decrease in temperature occurs simultaneously with a decrease in ET during the three different climatic events.

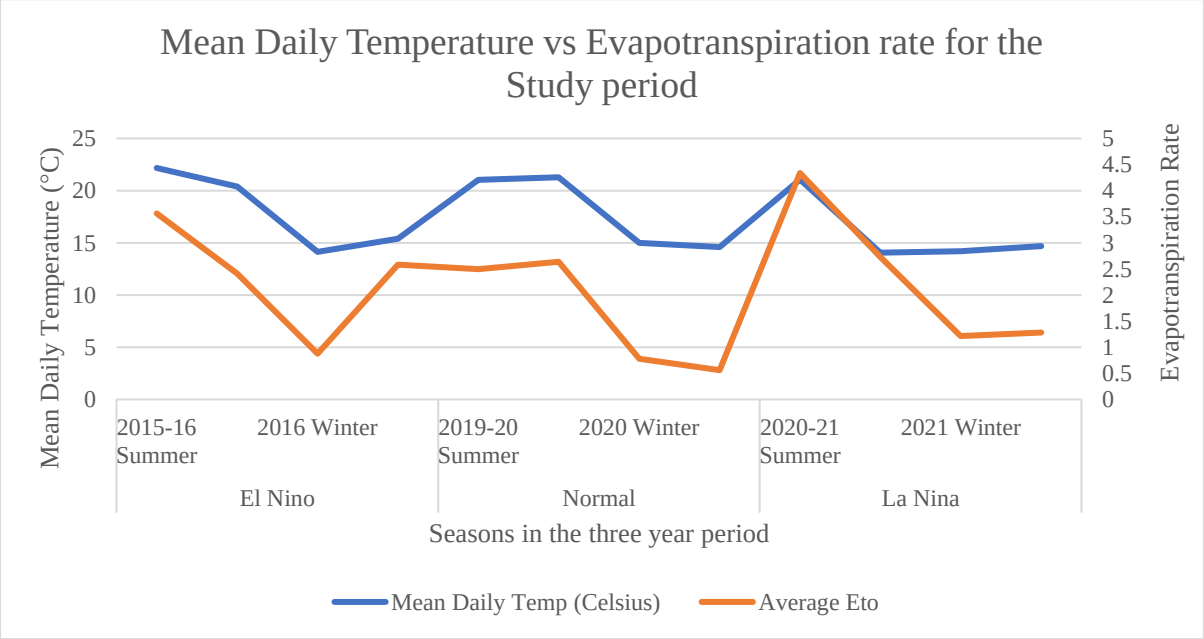

Figure 4.13: A graph showing the comparison between ET and mean daily temperature for El Nino in 2016, Normal in 2020, and La Nina in 2021.

Figure 4.14 is a graph that shows the relationship between ET and humidity for all three years. In general, this figure shows that the humidity between the three years seems to stay very similar with the major changes in humidity happening seasonal and not as much between different climatic events. There is also a relationship visible between ET and humidity because when humidity decreases, ET also decreases but the decrease in ET is much bigger than the increase in humidity.

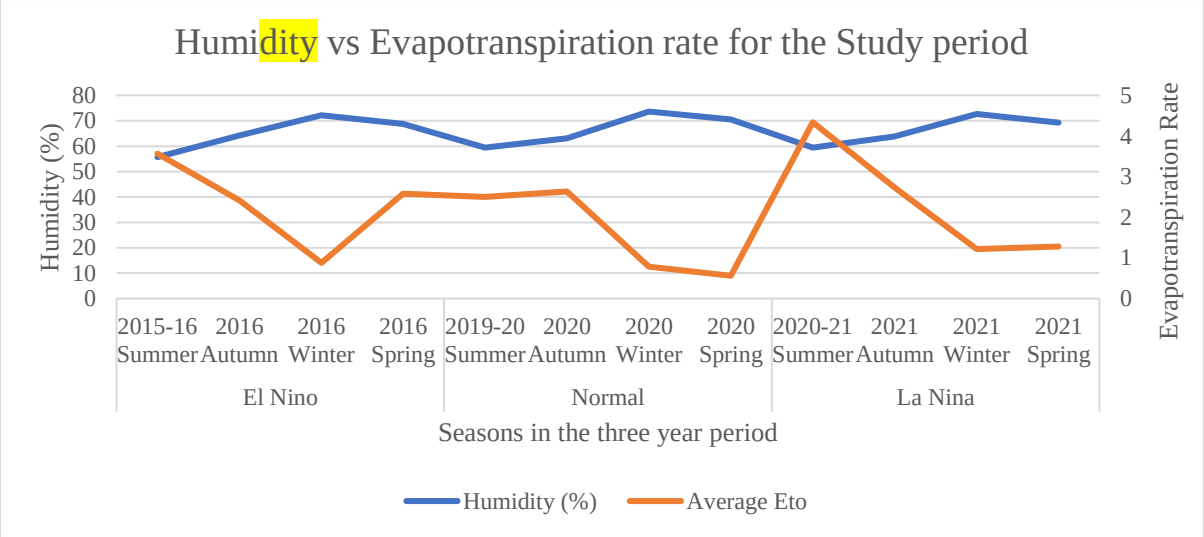

Figure 4.14: A graph showing the comparison between ET and humidity for El Nino in 2016, Normal in 2020, and La Nina in 2021.

Figure 4.15 shows a graph representing the comparison of wind speed versus ET rate for all three climatic events. Visually, the wind speed of the different years seems to be relatively similar with a bigger change in wind speed between the seasons than between the different climatic events. However, overall three climatic events, when a decrease in wind speed occurs, a decrease in ET also occurs.

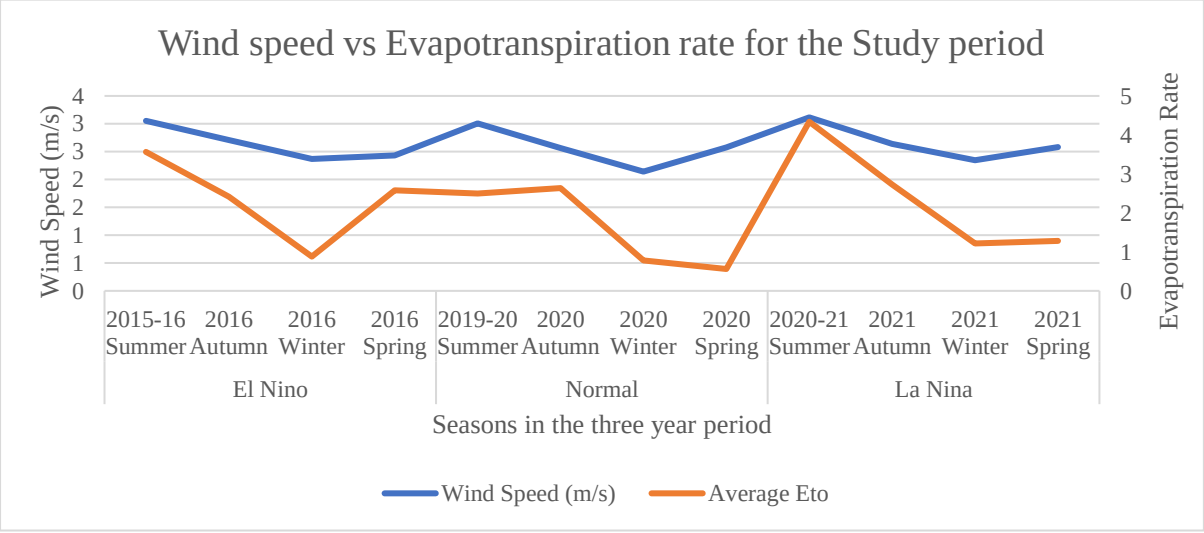

Figure 4.15: A graph showing the comparison between ET and wind speed for El Nino in 2016, Normal in 2020, and La Nina in 2021.

Figure 4.16 represents visually the comparison between surface pressure and ET rate. The surface pressure is lower in the La Nina years than in the other two years. However, the El Nino and normal years have similar surface pressures in similar seasons. A relationship between surface pressure and ET is not determined to exist when comparing the results visually.

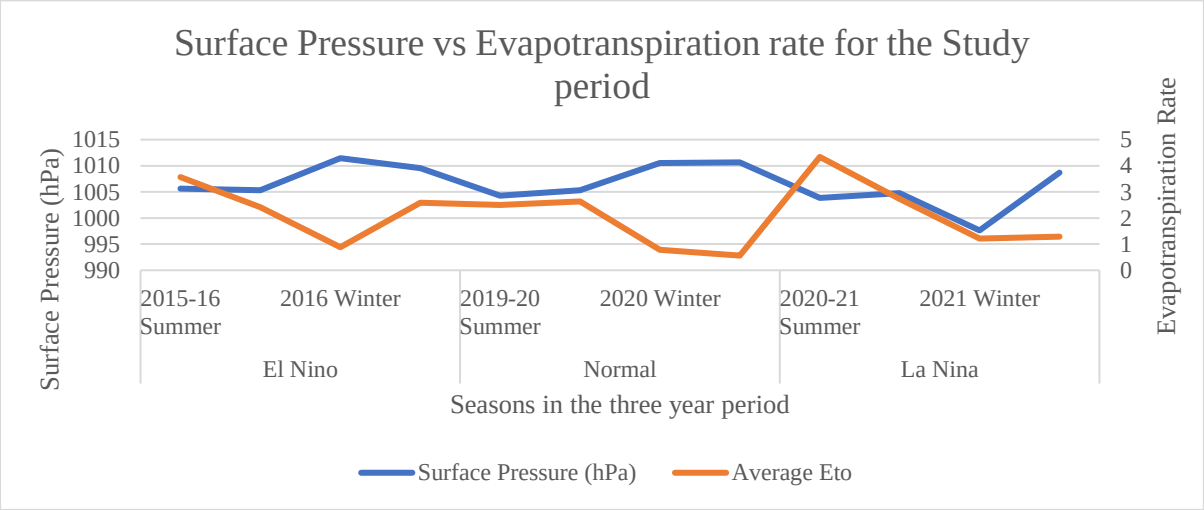

Figure 4.16: Graphs showing a comparison between ET and surface pressure for El Nino in 2016, Normal in 2020, and La Nina in 2021.

Table 4.4 shows the correlation between the different meteorological parameters and the ET rates through the R^2 values calculated using the Pearson correlation coefficient method. Where there is a higher R^2 value, there is a higher correlation which means that the bigger the difference in the meteorological parameter between the two climatic events that has the higher correlation, the greater the effect on the ET rate this parameter will have between the two climatic events. Based on the results represented in Table 4.3, the mean daily temperature has the strongest correlation (R^2 = 0.2535) followed by humidity (R^2 = -0.1142), then wind speed (R^2 = 0.0.369) and the weakest, with almost no correlation, is surface pressure (R^2=0.0172).

Table 4.4: The correlation between the meteorological data and the ET rates for the different seasons during El Nino in 2016, Normal in 2020, and La Nina in 2021.

Parameters	R^2 Value
Average ET vs Humidity	0.1142
Average ET vs Wind Speed	0.0369
Average ET vs Surface Pressure	0.0172
Average ET vs Mean Daily Temperature	0.2535

4.3 Assessing the variation in Land use land cover types across the study area

4.3.1 Spatial and temporal variations in LULC types from Landsat 8

The results of the land use land cover classification performed in this study using the Landsat 8 images are presented in Figure 4.17. Figure 4.17a and b are the El Nino summer and winter seasons, respectively Figure 4.17c and d are the La Nina summer and winter seasons. respectively. In general, across the study area, the different land use and land covers are roughly in the same area in both seasons in both years with the agricultural area being mainly in the middle of the northern section and spreading down the western side of the southern section of the study area. The grassland extends along the eastern side of the study area as well as a little on the far western and the far northern side of the study area. The built-up area is mostly in the south-south-western edge of the study area and scattered around the northern area of the study area. Shrubs were detected in small sections on the southern and eastern edges of the maps. The water bodies are also situated in roughly the same places across the seasons with the main water body being along the eastern side of the study area. Small areas of bare land were scattered throughout the agricultural section of the study area.

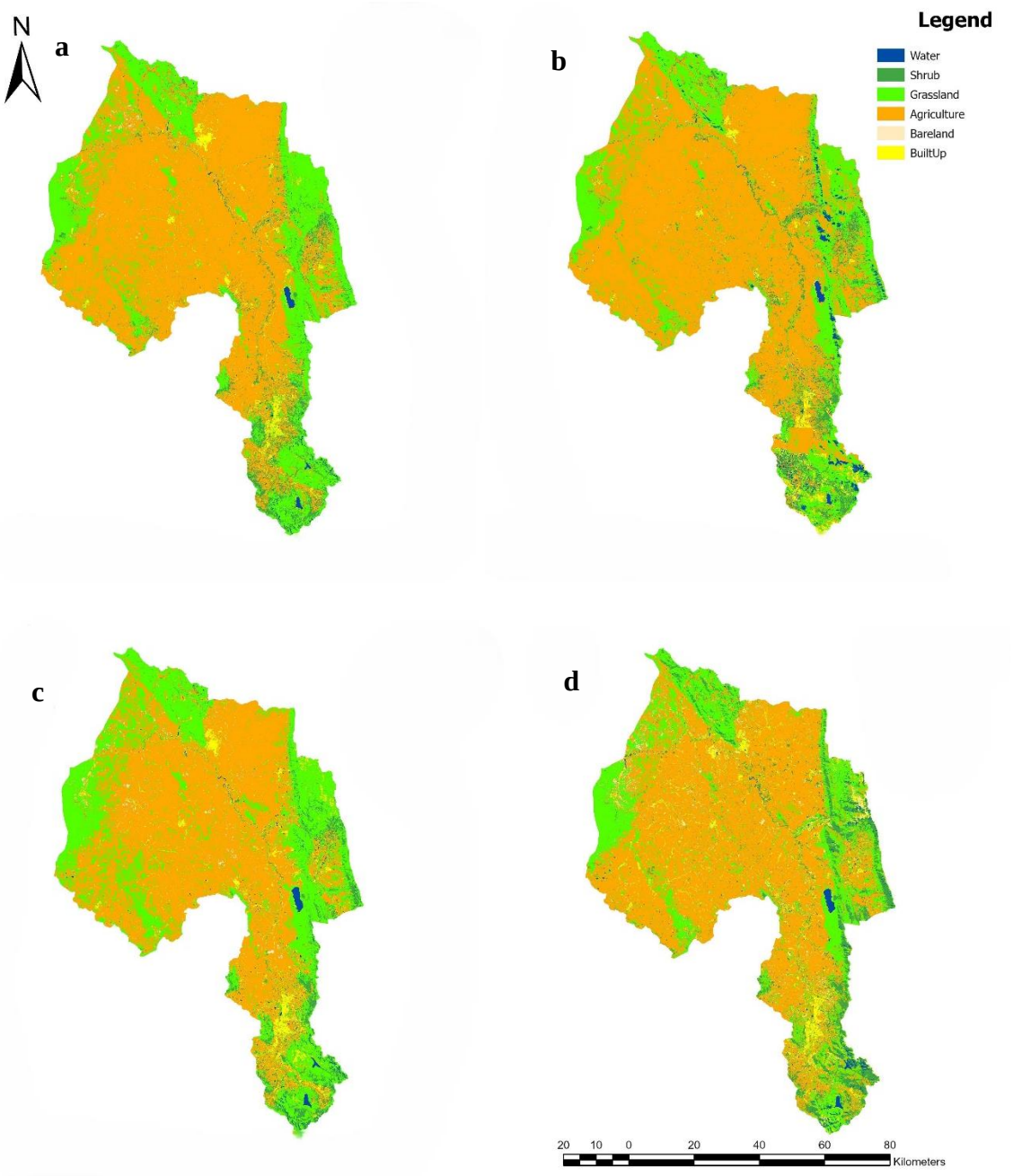

Figure 4.17: Seasonal distribution of the different LULC types of the study area during the El Nino (2015-2016) (Summer (a) and Winter (b)) and La Nina years (2020-2021) (Summer (c) and Winter (d)).

Table 4.5 shows the areal coverage of each LULC type as a percentage. These statistics show that agriculture covers most of the study area followed by grassland, shrubs, built-up, water, and bare land. There are more water bodies in the winter season than in the summer season when comparing the summer and winter images in the two years with an average of 1.64% of the study area being water bodies in the winter seasons compared to 0.83% in the summer

season. There was more shrubland cover in the winter seasons than in the summer seasons with an average coverage of the study area of 6.73% and 4.79% respectively. When comparing the El Nino with the La Nina years, there was less agricultural land and more grassland in the La Nina year (average coverage of 59.62% and 27.56% respectively) than in the El Nino year (average coverage of 66.13% and 24.49% respectively). The built-up area in the southern section of the map has also expanded from 2015-2016 to 2020-2021 with an average coverage of the study area going from 2.52% to 4.43%.

Table 4.5: Seasonal areal coverage for the different LULC types for the El Nino (2015/16) and La Nina (2020/21) years.

LULC classes	**Percent of study area covered by LULC (%)**			
	Summer 2015/16	**Winter 2016**	**Summer 2020/21**	**Winter 2021**
Water	0.73	2.02	0.92	1.25
Shrub	5.30	5.32	4.27	8.14
Grassland	26.02	22.96	32.27	22.85
Agriculture	65.04	67.21	57.85	61.38
Bare land	0.23	0.14	0.56	1.65
Built-Up	2.68	2.35	4.13	4.73

4.3.2 LULC classification accuracy assessment

A confusion matrix accuracy assessment was performed on each of the LULC classifications that were performed. Each of these confusion matrices can be found in full in Appendix 1. The summarized producer, user, and overall accuracies as well as the kappa statistics can be found in Table 4.6. The overall accuracy of the classification was very good with the highest accuracy being 94% with a kappa statistic of 0.928 for Summer 2015-16 and the lowest accuracy being in Winter 2021 with 86% and a kappa statistic of 0.832. The class that was classified with the highest accuracy was the water class which has 100% User accuracy in both summer seasons and above 87% accuracy across all seasons and years. The class with the lowest accuracy is the agricultural class, especially in the summer season of 2020-21 where the user and producer accuracies were only 78%. However, overall, on average the accuracy for all classes was above 80%. This shows that the accuracies of the LULC are very good and can be used in this study for further analysis.

Table 4.6: A table showing the summarized accuracies and Kappa statistics for the LULC assessments performed.

Classes		Water	Shrub	Grassland	Agriculture	Bare land	Built-up
Summer 2015-16	**Producer Accuracy**	0.9700	0.9091	0.9406	0.9200	0.9400	0.9600
	User Accuracy	1.0000	0.9474	0.9500	0.8762	0.9495	0.9231
	Overall Accuracy	**0.94**					
	Kappa Statistic	**0.928**					
Winter 2016	**Producer Accuracy**	0.9495	0.9802	0.7700	1.0000	0.9500	0.7800
	User Accuracy	0.9592	0.9000	0.8750	0.8000	0.9794	0.9512
	Overall Accuracy	**0.905**					
	Kappa Statistic	**0.886**					
Summer 2020-21	**Producer Accuracy**	0.9600	0.9400	0.9400	0.7800	0.8400	0.9700
	User Accuracy	1.0000	0.9691	0.9126	0.7879	0.9545	0.8291
	Overall Accuracy	**0.905**					
	Kappa Statistic	**0.886**					
Winter 2021	**Producer Accuracy**	0.8700	0.9800	0.9200	0.7700	0.7100	0.9100
	User Accuracy	0.9063	0.8909	0.7863	0.8556	0.9342	0.8198
	Overall Accuracy	**0.86**					
	Kappa Statistic	**0.832**					

4.4 Assessing the SEBS-derived ET variations for the different LULC classes

Table 4.7 shows the results of zonal statistics performed using ArcGIS to calculate the median of each land cover class for each summer and winter season in each of the three years. The same LULC created for 2020-2021 was used in the 2019-2020 year as the LULC does not change drastically enough to require the need to create another LULC map for this year. Overall, the average ET rate for the Summer 2015-16 season is higher (3.5722mm/day) than the summer 2020-21 season (3.4317mm/day), and both the climatic event years have a higher average ET rate for the LULC covers than the normal year (3.351mm/day). However, the average ET rate for the winter 2016 image is lower (0.6280mm/day) than the winter 2021 image (0.6367mm/day) and the normal year is higher (0.7880mm/day) than both climatic event years.

In individual classes, the class with the highest ET rate in most of the images for each season (summer and winter 2016, summer 2020 as well as summer 2021) is agriculture with it being the second highest in the winter 2020 and 2021 seasons (the highest is grassland for this season for these 2 years). The class with the lowest ET rate is the same in all seasons and all years and is the water bodies class. The results show that in the El Nino year, in summer the average ET

rate for the individual classes is higher than in winter and higher than in the La Nina year, but the winter season has a lower ET rate for the individual classes in the El Nino year than the La Nina year. The normal year has a lower average Eto in the summer season and a higher average Eto in the winter season when compared to both climatic events.

Table 4.7: A table showing the ET for each LULC type in the summer and winter seasons for the three years. (Min, Max)

Summer 2015-16 LULC SEBS value		
Class Name	**Class Value**	**ET Median**
Water	10	2.8090
Shrub	20	3.6710
Grassland	30	3.6880
Agriculture	40	3.8350
Bareland	50	3.6360
Built-up	60	3.7940
Average		**3.5722**

Winter 2016 LULC SEBS value		
Class Name	**Class Value**	**ET Median**
Water	10	0.5770
Shrub	20	0.6580
Grassland	30	0.6750
Agriculture	40	0.6850
Bareland	50	0.5830
Built-up	60	0.5900
Average		**0.6280**

Summer 2019-20 LULC SEBS value		
Class Name	**Class Value**	**ET Median**
Water	10	2.7250
Shrub	20	3.1900
Grassland	30	3.4910
Agriculture	40	3.6250
Bareland	50	3.5640
Built-up	60	3.5110
Average		**3.3510**

Winter 2020 LULC SEBS value		
Class Name	**Class Value**	**ET Median**
Water	10	0.7010
Shrub	20	0.7560
Grassland	30	0.8330
Agriculture	40	0.8290
Bareland	50	0.7980
Built-up	60	0.8110
Average		**0.7880**

Summer 2020-21 LULC SEBS value		
Class Name	**Class Value**	**ET Median**
Water	10	2.6510
Shrub	20	3.2410
Grassland	30	3.6730
Agriculture	40	3.7620
Bareland	50	3.6470
Built-up	60	3.6160
Average		**3.4317**

Winter 2021 LULC SEBS value		
Class Name	**Class Value**	**ET Median**
Water	10	0.5980
Shrub	20	0.6270
Grassland	30	0.6640
Agriculture	40	0.6590
Bareland	50	0.6310
Built-up	60	0.6410
Average		**0.6367**

4.5 Summary of the Chapter

This section presented the results of the research done and achieved the aim of determining the ET rates of different LULC classes and the effects of climatic phenomena on ET. The results from the SEBS model were illustrated in the form of multiple maps showing the spatial variation of ET rates within the study area for each season for the two different climate events (El Nino and La Nina years) in 2015-2016 and 2020-2021 and for the Normal year, 2019-2020.

The results show that the El Nino and La Nina years have higher ET rates than the normal year. It is also noted that in general there is seasonal variation between ET rates with the summer seasons having the highest average ET rates, the winter season having the lowest ET rates, and the autumn season having a higher average ET than the spring season. The SVM classification was performed to determine the LULC of the study area for the 2015/2016 and 2020/2021 years. In general, across the study area, the different land use and land covers are roughly in the same area in both seasons in both years with agriculture covering most of the study area followed by grassland, shrubs, built-up, water, and bare land. Using the LULC classifications a comparison was made of the ET and the different LULC classes to determine what the effect of the different classes are on the ET rate. The results of this comparison show that agriculture has the highest ET rate in most of the seasons, with some seasons having grassland with the highest ET rate and the water bodies class has the lowest ET rate in all the years seasons. These results are discussed in more detail, referring to relevant supporting literature, in the next chapter.

CHAPTER FIVE: DISCUSSIONS

5.1 Introduction

This chapter focuses on the discussion of the results by discussing the three objectives of this study. The main results are presented, explained, and linked to the findings of other studies. The limitations of the study are highlighted and recommendations for future studies are based on the limitations suggested. The study is also summarized in this chapter and concluding remarks are mentioned.

5.2 Seasonal variation in SEBS-derived ET estimations during the different climatic events

For the general overall ET rate for the study area, the climatic events have a higher ET than the normal year. This could be because in the El Nino year, there were increasing temperatures which would increase the ET rate and in the La Nina year there was increasing rainfall which resulted in more water available to be evaporated, thereby increasing ET (Shikwambana and Kganyago, 2023; Shikwambana *et al.,* 2023). Although a study done by Botai *et al.,* (2017), did not specifically link ET to the ENSO events, they found that the decrease in rainfall and increase in warm temperatures caused in the El Nino year 2015-2016 in comparison to normal years, increased the ET rate. This increase in ET rate caused more water stress issues in crops as well as loss of water in reservoirs. Botai *et al.* (2017) therefore, agree with the results of this study that the La Nina and El Nino climatic events affect the ET rates due to the climatic events affecting the various meteorological data.

The results of this study show a relationship between temperature, rainfall, and ET as mentioned with the El Nino year experiencing increasing temperatures and ET rate and the La Nina year experiencing increasing rainfall and ET rate. Zhang *et al.,* (2001) and Zhang *et al.,* (2004) state that although ET is a complex process with many interactions associated with it, the availability of water and energy have been shown to have primary effects on ET with the key controls on ET being rainfall interception, turbulent transport, net radiation, advection, plant-available water capacity and leaf area. This study agrees with this statement through the results showing that the availability of water through rainfall in the La Nina year has a primary effect on ET and the availability of energy through temperature has a primary effect on ET in the El Nino year. What this also suggests is that this catchment area is both energy-limited and water-limited (Zhang *et al.,* 2004). With a lack of water in the El Nino year, the ET rate is

limited by the availability of water as the increased temperature is in abundance and driving the ET rate. However, in the La Nina year, the increase in water available through increased rainfall, results in the ET rate being limited by the energy available for ET to occur as the amount of water is in abundance. However, this was not the focus of this study and it is recommended that future studies are done within this study area to confirm this observation.

The overall ET rate for all four seasons for the two climatic events showed that the average ET of all these seasons in the La Nina year is higher than the El Nino year seasons. As mentioned previously, as far as is known, little to no studies have been done on the effects of the El Nino and La Nina climatic events on ET rates. However, there have been studies done on the effect of rainfall on ET (Cui *et al.*, 2022). Cui *et al.* (2022) found that excessive light rain can cause an underestimation of evaporation and transpiration using the normal global climate models (GCMs). When there is excessive light rain, there is an increase in ET as the surface becomes saturated resulting in more water available for evaporation. Due to the characteristics of the rainfall in the study area, the La Nina year increases the light rain experience in this area when compared to a normal year. The findings of the study by Cui *et al.* (2022) could then potentially explain why the La Nina year could have a greater ET rate in comparison to the El Nino year as although the drought years increased temperatures when compared to the normal year which increases ET, the increased light rainfall in La Nina years also increases the ET in comparison to the normal year. This increase in the La Nina year could be greater than the increase experienced in the El Nino year (Cui *et al.*, 2022)**.** A different study would need to be performed comparing more El Nino and La Nina climatic events to confirm if this is an explanation for the difference.

The effect of the climatic events can also be seen in the different seasons, the La Nina event has a higher ET rate in the images acquired in the summer, autumn, and winter seasons and a lower ET rate in the images acquired in the spring season when compared to the El Nino year. This shows that even when looking at the individual seasons, the La Nina year has more seasons with higher ET rates than the El Nino year. This highlights that it is possible that the increasing of rainfall increases ET more than the increasing of temperatures with decreasing rainfall as explained by the study done by Cui *et al.* (2022) mentioned previously.

Although climatic events do affect the ET rates, the different seasons affect the ET rates more than the climatic events. The results in this study show the summer season in all the years had

a higher ET rate than all the other seasons, the winter season had the lowest ET rate, and the autumn season had a slightly higher ET rate than the spring season. Seasonal variation has been proven to greatly affect the ET rate by many different authors in many different study areas (Palmer and Weideman, 2011; Majozi *et al.,* 2017; Dzikiti *et al.,* 2019). For this study area the summer image showing the highest ET rate agrees with findings by Jovanovic *et al.* (2014) who stated that due to the characteristics of the winter rainfall in the Western Cape, increased sunshine hours, wind speed, and temperatures in the summer, the ET rate is higher in the summer.

Although there is a difference between the normal year and climatic events ET, it is very small. The variation of the different meteorological parameters for the different climatic events is also very slight. By nature, ET is affected by different meteorological parameters (Elhag *et al.,* 2011; Botai *et al.,* 2017; Veste *et al.,* 2020). Therefore, the lack of major difference between the climatic events and the normal year could be explained by the lack of variation between the meteorological parameters for these years. For example, a study done by Cui *et al.* (2022) showed that increased rainfall can strongly affect ET by comparing different GCMs.

This study also proved that different meteorological parameters affect ET based on Pearson's correlation. The correlation performed in this study showed that the mean daily temperature had the strongest correlation followed by humidity which had a negative correlation. Therefore, the higher the temperature the higher the ET rate, and the higher the humidity the lower the ET rate. This would then explain why the results in this study showing that the climatic events do affect the ET rates would be accurate as these events do strongly affect the temperature and humidity during the period they occur through increased temperatures and decreased rainfall in the El Nino events and increased rainfall in the La Nina events (Harduth and Fitchett, 2020; Shikwambana *et al.,* 2023). Many studies have been done to determine the sensitivity of ET to various meteorological parameters and a study by Ali *et al.* (2009) agreed with the findings of this study that temperature has the greatest effect on ET, followed by humidity. Ali *et al.* (2009) proved these results that agree with this study by doing a sensitivity analysis using the PMequation in a region in Bangladesh.

The RMSE calculated in this study shows that the accuracy of the SEBS model is very low when compared to the results of the Reference ET with an average RMSE of 56.63% for the study area. This is potentially because only three weather stations were used for the SEBS

model meteorological data making generalized ET values for the rest of the study area based on the meteorological data from the three weather stations. A study done by Rwasoka *et al.* (2011) also found that the average accuracy of the SEBS ET was low especially the further away from the weather station the ET rate was estimated. This was discovered by studying the ET rates using MODIS satellite imagery and the SEBS model in the Upper Manyame catchment in Zimbabwe (Rwasoka *et al.*, 2011).

When comparing the differences between the ET rates of the reference data and the SEBS model visually, the effect of the weather stations on the results of the reference ET is shown based on the maps looking like wind speed interpolated maps. This shows that the reference ET is strongly affected by the placement of the weather stations, and this might mean that the reference ET is the inaccurate variable and not the SEBS model ET. Singh and Senay (2015) also stated that although their study assumed that the inaccuracies between the estimated ET and the observed ET were with the models, the reference ET can be the cause of the issues due to incorrect collection of data, instrument sampling errors, and other random observation errors. This was determined when comparing four SEB models (METRIC, SEBAL, SEBS, and SSEBop) using Landsat images in the Midwestern United States and agrees with the findings in this study where the reference ET is showing a spatial distribution more similar to a wind interpolated map than ET rates of different LULC within the study area (Singh and Senay (2015).

5.3 Assessing the variation in Land use land cover types across the study area

The LULC classification of this study showed that agriculture covers over half of the study area followed by grassland, shrubs, built-up, water, and bare land. The reason this area is so rich in agriculture is because its Mediterranean-type climate is extremely ideal for grape cultivation as well as other fruit and vegetables (Zwane, 2019). Due to the amount of agricultural land in the study area and the broader area around the study area, Talanow *et al.* (2021) conducted a study to determine the farmer's strategies for adaptation and perceptions of climate change in this area. This highlights the extent of the agricultural land in this study area. Talanow *et al.* (2021) also state that the province that this study area is in accounts for 12% of the total agricultural land within South Africa.

The variation of LULC of the study area between the two seasons is very slight with the biggest difference being in the grassland class where the summer season was shown to have an average of 6.24% more grassland than the winter season. This shows that the LULC does not change that much between seasons. An explanation for this lack of variation is that the seasons might affect the crops that are growing or the healthiness of the shrub, but the actual LULC type will still be the same, the spectral signature for the seasons might just be a little different. Sinha *et al.* (2012) agree with this statement that the spectral signatures for the LULC classes are different for different seasons and performed a study to determine the effect of seasonal variation on the accuracy of LULC classification.

The difference between the LULC coverage between climatic events is also minimal with the biggest difference being in the agriculture class where the average coverage is 6.51% more in the El Nino year compared to the La Nina year. This highlights that the climatic events affect the spatial distribution of the LULC classes minimally. These events in general are not the main causes of LULC changes but rather phenomena like urbanization, population growth, and anthropogenic activities in general cause the LULC to change over time (Chughtai *et al.*, 2021).

The SVM classification method used in this study had a very high overall accuracy for all the classifications with the highest being 94% and the lowest being 86%. This shows that the LULC classification for this study was very accurate and using the SVM method was a suitable method for the study area in this study. Basheer *et al.* (2022) compared different classification methods (SVM, MLC, RF, minimum distance, and classification and regression tree) in Charlottetown, Canada using Landsat, Sentinel, and Planet satellite imagery. The SVM classifier was found to have the best performance over all the other classifiers with all the satellite images with an overall average accuracy of 92% (Basheer *et al.,* 2022). This agrees with the findings of this study that the SVM classification can accurately determine changes in LULC types over time.

5.4 Assessing the SEBS-derived ET variations for the different LULC classes

There was a variation between the ET rates of the different LULC classes. This shows that the different LULC classes do affect the ET rates of the catchment area, highlighting how understanding the different LULC classes can help create a better understanding of the ET rates and therefore be able to create better management plans**.** Studies in other areas within and

outside of South Africa agree with these results and state that it is a general understanding that LULC will affect the ET rates but the exact dynamics of this are unknown (Gwate *et al.,* 2018a; Odongo *et al.,* 2019). Gwate *et al.* (2018a) found that LULC affected ET based on the change of the evaporative index and confirmed this through the catchment parameter dynamics in the study. The study area for the study was a quaternary catchment area S50E in South Africa and used MODIS imagery, meteorological ground-based data, and already-made LULC maps from the National Land Cover (NLC) (Gwate *et al.,* 2018b). Odongo *et al.* (2019) used MODIS imagery, ground-based meteorological data, and the SEBS model to determine ET for different LULC classes in Lake Naivasha Basin, Kenya, and found that the changing of the LULC did affect the rate of ET up to 12% for some of the changes.

The water bodies had the lowest ET rate for all the images in the summer and winter seasons in all the years. Water bodies take longer to heat up than other land surfaces due to the absorption of heat by water. ET is greatly affected by temperature, humidity, and wind. The higher the temperature of the water the greater the ET, proven in this study by the correlation between temperature and ET. This could be a possible explanation for the low ET of this LULC type in comparison to the other LULC types. Different studies have found mixed findings related to ET rates from water bodies. For example, Gyamfi *et al.* (2016) found that other LULC types had greater effects on the ET than the water bodies class by using Landsat 7 images and the Soil and Water Assessment Tool (SWAT) within the study area of Olifants Basin in South Africa. A study by Liu *et al.* (2010) however, found that the water bodies class had the highest ET rate when compared to wetland, forest, grassland, and agricultural lands in central Oklahoma using Landsat 5 imagery, ground-based meteorological data, and the SEB method. Lie *et al.* (2010) determined that the greater the amount of water available in the LULC type, the greater the ET. However, central Oklahoma is in a different country with different weather characteristics that could explain the contradiction to the results found in this study.

Agriculture had a strong effect on the ET rate as, except for the winter season of 2020 and 2021, this class had the highest ET rate. In the winter seasons of 2020 and 2021, grassland had the highest ET rate, followed very closely by agriculture. In the other classes, although the ET rate does differ for the different seasons and years, the difference is not consistent. This shows that their effect on the ET rate is not as consistent or strong as the other three classes. A potential reason for the increase in ET rate over agricultural LULC is the increase in water use through irrigation. If incorrect irrigation practices are followed, there would be an excess of water to be

evaporated. For example, if the crops are irrigated in the middle of a sunny day, the ET rate would increase as the water evaporates relatively quickly (i.e. sometimes even before it is absorbed into the soil or by the plant). The fact that agriculture had such a strong effect on ET was also found by Odongo *et al.,* (2019) who discovered that increasing agricultural lands greatly increased the ET rate. When the LULC changed to grassland from agriculture the ET rate decreased. This agrees with the results that agricultural land cover had the highest ET rate and therefore, proper water management plans in this LULC will reduce water lost through ET.

Broadly comparing the effect that climatic events have on the LULC's effect on ET rates, the El Nino summer season had a higher average overall ET rate for the different classes than the La Nina summer season, but the La Nina winter season had a higher average overall ET rate for the different classes than the El Nino winter season. A possible explanation for this is the increased temperature of the El Nino event could cause more ET in different LULC types in the summer season but the increased rainfall in the La Nina winter season (the study areas' rainy season) results in more ET in the LULC classes during this climatic event for this season (Jovanovic *et al.,* 2014; Bhaga *et al.,* 2021). This also suggests that the ET rate in this catchment area is more limited by water than by energy as mentioned previously.

5.5 Limitations

This study showed that the ET rates can be accurately determined using the SEBS model for different seasons and different climatic events and that the SVM LULC classification can accurately determine the LULC of the study area to be able to compare the ET rates of different LULCs and different climatic events. However, there were some limitations to the methods followed in this study. Only one image was used for each season to determine the ET of the season due to the limitations of the combination of the temporal resolution for Landsat 8 and the cloud cover in the season. This might create bias and misrepresent the seasons as only one image is used instead of multiple to find an average for the season. With regards to comparing the different climatic events, using only one year for each event could result in bias when trying to determine a trend of what the effect of the climatic events had on the ET rates.

There were only three weather stations used that were within the study area making the meteorological data that was used relatively generalized for most of the study area. Having more weather stations could result in more accurate meteorological data used for the SEBS

model and the reference ET which could lead to better ET results. However, this was ameliorated by making sure the data received from the weather station was complete and the most accurate weather stations were chosen. The SEBS model, although freely available, requires many different inputs which must be processed before the model can be used and put into the same projection, make sure the units are correct, etc. This can present inaccuracies, however, in this study, extreme care was taken that all transformations were done correctly and as accurately as possible. If more images are used for each season, this could become more tedious and time-consuming and open for more errors when processing the images for the model making the results inaccurate. The validation of the ET rates calculated using the SEBS model was done using another model instead of only ground-truth data, this could present inaccuracies in the validation of the data, this limitation was ameliorated by doing both a statistical and visual-spatial distribution analysis of the datasets.

5.6 Conclusions

Evapotranspiration is a major contributor in which water that is available for use in a water resource is converted by heat into vapor and transferred into the atmosphere making it an important phenomenon to understand, to create better water resource management plans in semi-arid regions. Climatic events are known to affect the meteorological data that affects the rate of evapotranspiration so understanding how these events affect evapotranspiration allows for more information to be collected about the rate at which water is being lost through evapotranspiration. Using Landsat 8 images and meteorological data from a catchment area within the Western Cape, the evapotranspiration rates and different LULC types of the study area were determined, and it was determined whether different LULC classes affect the evapotranspiration rates and whether the different climatic events affect the evapotranspiration rates of the study area. The SEBS model was used to determine the evapotranspiration rates using Landsat 8 images. The study covered four seasons during El Nino 2015-2016 and La Nina 2020-2021 as well as during the normal year of 2019-2020. The study also assessed LULC using the Landsat 8 and the SVM advanced machine learning classifier. The study successfully determined that climatic events and different LULC types do affect evapotranspiration rates in different ways. Evapotranspiration rates increased when both climatic events occurred when compared to a normal year. However, the La Nina climatic event increases the evapotranspiration more than the El Nino climatic event in all seasons, except for the spring season. Concerning the different LULC cover types, overall, on average for all the

seasons in the three years, the water class had the lowest ET whereas the agricultural class had the highest evapotranspiration. In conclusion, El Nino and La Nina climatic events increase the ET in comparison to the normal year and the LULC type does cause variation in the evapotranspiration rates with the water class having the lowest evapotranspiration and the agricultural class having the highest.

5.7 Recommendations

- Future studies may consider covering more extreme events to understand ET dynamics. Using more than one year could help determine in a more generalized manner whether all El Nino and La Nina events affect ET.
- Choosing a different satellite, for example, MODIS imagery, would result in a lower spatial resolution but a higher temporal resolution. More than one image could be used for each season if MODIS imagery was used resulting in a more accurate average ET for each season being determined.
- Using data integration or fusion using the MODIS ET product instead of the SEBS modeling could result in more accurate ET estimations.
- Including more weather stations or identifying other sources of meteorological data to include more ground-based data could result in more accurate reference ET as well as SEBS ET.

REFERENCES

Abid, N., Mannaerts, C. and Bargaoui, Z. 2019. Sensitivity of actual evapotranspiration estimation using the SEBS model to variation of input parameters (LST, DSSF, aerodynamics, parameters, LAI, FVC). *The International Archives of the Photogrammetry, Remote Sensing and Spatial Information Sciences,* 42(2), 1193–1200.

Abrishamkar, M. and Ahmadi, A. 2017. Evapotranspiration estimation using remote sensing technology based on SEBAL algorithm. *Iran Journal of Science and Technology, Transactions of Civil Engineering,* 41, 65–76.

Ali, M.H., Adham, A.K.M., Rahman, M.M. and Islam, A.K.M.R. 2009. Sensitivity of Penman-Monteith estimates of reference Evapotranspiration to errors in input climatic data. *Journal of Agrometeorology,* 11(1), 1–8.

Allen, R.G., Pereira, L.S., Raes, D. and Smith, M. 1998. Crop Evapotranspiration – Guidelines for computing crop water requirements FAO irrigation and drainage paper 56. Food and Agriculture Organization of the United Nations, Rome, Italy, 15–64.

Apaydin, H., Sonmez, F.K. and Yildirim, S.Y. 2004. Spatial interpolation techniques for climate data in the GAP region in Turkey. *Climate Research,* 28, 31–40.

Basheer, S., Wang, X., Farooque, A.A., Nawaz, R.A., Liu, K., Adekanmbi, T. and Liu, S. 2022. Comparison of land use land cover classifiers using different satellite imagery and machine learning techniques. *Remote Sensing,* 14, doi:10.3390/rs14194978.

Bhaga, T.D., Dube, T. and Shoko, C. 2021. Satellite monitoring of surface water variability in the drought prone Western Cape, South Africa. *Physics and Chemistry of the Earth*, 124, 102914.

Botai, C.M., Botai, J.O., de Wit, J.P., Ncongware, K.P. and Adeola, A.M. 2017. Drought characteristics over the Western Cape province, South Africa. *Water,* 9(876), doi:10.3390/w9110876.

Bronnimann, S., Xoplaki, E., Casty, C., Pauling, A. and Luterbacher, J. 2007. ENSO influence on Europe during the last centuries. *Climate Dynamics,* 28, 181–197.

Chughtai, A.H., Abbasi, H. and Karas, I.R. 2021. A review on change detection method and accuracy assessment for land use land cover. *Remote Sensing Applications: Society and Environment,* 22, 100482.

Coulibaly, M. and Becker, S. 2007. Spatial interpolation of annual precipitation in South Africa – a comparison and evaluation of methods. *Water International,* 32(3), 494–502.

Cui, Z., Wang, Y., Zhang, G.J., Yang, M., Liu, J. and Wei, L. 2022. Effect of improved simulation of precipitation on evapotranspiration and its partitioning over land. *Geophysical Research Letters,* 49, doi:10.1029/2021GL097353.

Department of Environmental Affairs and Development Planning. 2011. Land use. In: *Western Cape IWRM Action Plan: Status Quo Report Final Draft.* Western Cape, 312–327.

Dzikiti, S., Schachtschneider, K., Naiken, V., Gush, M. and Le Maitre, D. 2013. Comparison of water-use by alien invasive pine trees growing in riparian and non-riparian zones in the Western Cape Province, South Africa. *Forest Ecology and Management,* 293, 92–102.

Dzikiti, S., Jovanovic, N.Z., Bugan, R.D.H., Ramoelo, A., Majozi, N.P., Nickless, A., Cho, M.A., le Maitre, D.C., Ntshidi, Z. and Pienaar, H.H. 2019. Comparison of two remote sensing models for estimating evapotranspiration: algorithm evaluation and application in seasonally arid ecosystems in South Africa. *Journal of Arid Land,* 11(4), 495–512.

Elhag, M., Psilovikos, A., Manakos, I. and Perakis, K. 2011. Application of the SEBS water balance model in estimating daily evapotranspiration and evaporative fraction from remote sensing data over the Nile Delta. *Water Resources Management,* 25, 2731–2742.

Elkatoury, A., Alazba, A.A. and Mossad, A. 2020. Estimating evapotranspiration using coupled remote sensing and three SEB models in an arid region. *Environmental Processes,* 7, 109–133.

Esmail, M., Masria, A. and Negm, A. 2016. Monitoring land use/land cover changes around Damietta Promontory, Egypt, using RS/GIS. *Procedia Engineering,* 154, 936–942.

Fahdawi, Y.M.N.A., Ramahi, F.K.M.A. and Alfalahi, A.S.H. 2021. Measurement albedo coefficient for land cover (lc) and land use (lu), using remote sensing techniques, a study case: Fallujah city. *Journal of Physics: Conference Series,* 1829, 012003.

Generoso, R., Couharde, C., Damette, O. and Mohaddes, K. 2020. The growth effects of El Nino and La Nina: local weather conditions matter. *Annals of Economics and Statistics,* 140, 83–126.

Ghaderi, A., Dasineh, M., Shokri, M. and Abraham, J. 2020. Estimation of actual evapotranspiration using the remote sensing method and SEBAL algorithm: a case study in Ein Khosh Plain, Iran. *Hydrology,* 7(36), doi:10.3390/hydrology7020036.

Gibson, L., Munch, Z., Carstens, M. and Conrad, J. 2011. *Remote sensing Evapotranspiration (SEBS) evaluation using water balance.* Report to the Water Research Commission, Stellenbosch.

Gibson, L.A., Munch, Z. and Engelbrecht, J. 2011. Particular uncertainties encountered in using a pre-packaged SEBS model to derive evapotranspiration in a heterogeneous study area in South Africa. *Hydrology and Earth System Sciences,* 15, 295–310.

Gibson, L.A., Jarmain, C., Su, Z. and Eckardt, F.E. 2013. Estimating evapotranspiration using remote sensing and the Surface Energy Balance System – A South African perspective. *Water South Africa,* 9(4), 477–484.

Grimm, A.M., Barros, V.R. and Doyle, M.E. 2000. Climate variability in southern South America associated with El Nino and La Nina events. *Journal of Climate,* 13, 35–58.

Gwate, O., Mantel, S.K., Gibson, L.A., Munch, Z. and Palmer, A.R. 2018. Exploring dynamics of evapotranspiration in selected land cover classes in a sub-humid grassland: a case study in quaternary catchment S50E, South Africa. *Journal of Arid Environments,* 157, 66–76.

Gwate, O., Mantel, S.K., Palmer, A.R., Gibson, L.A. and Munch, Z. 2018. Measuring and modeling evapotranspiration in a South African grassland: comparison of two improved Penman-Monteith formulations. *Water SA,* 44(3), 482–494.

Gyamfi, C., Ndambuki, J.M. and Salim, R.W. 2016. Hydrological responses to land use/cover changes in the Olifants Basin, South Africa. *Water,* 8(588), doi:10.3390/w8120588.

Harduth, T. and Fitchett, J.M. 2020. Climatic deviations across a transect of South Africa during El Nino and La Nina years. *Journal of Climate Change Research,* 1(4), 49–65.

Hassan, A., Ismail, S.S., Elmoustafa, A. and Khalaf, S. 2018. Evaluating evaporation rate from high Aswan Dam Reservoir using RS and GIS techniques. *The Egyptian Journal of Remote Sensing and Space Sciences,* 21, 285–293.

Haung, C., Li, Y., Gu, J., Lu, L. and Li, X. 2015. Improving estimation of evapotranspiration under water-limited conditions based on SEBS and MODIS data in arid regions. *Remote Sensing*, 7, 16795–16814.

Hofstra, N., Haylock, M., New, M., Jones, P. and Frei, C. 2008. Comparison of six methods for the interpolation of daily European climate data. *Journal of Geophysical Research,* 113, doi:10.1029/2008JD010100.

Huo, Z., Dai, X., Feng, S., Kang, S. and Huang, G. 2013. Effect of climate change on the reference evapotranspiration and aridity index in arid region of China. *Journal of Hydrology,* 492, 24–34.

Jawak, S.D., Devliyal, P. and Luis, A.J. 2015. A comprehensive review on pixel oriented and object-oriented methods for information extraction from remotely sensed satellite images with a special emphasis on cryospheric applications. *Advances in Remote Sensing*, 4, 177–195.

Jovanovic, N., Garcia, C.L., Bugan, R.D.H., Teich, I. and Garcia Rodriguez, C.M. 2014. Validation of remotely-sensed ET and NDWI using ground measurements at Riverlands, South Africa. *Water South Africa,* 40(2), 211–220.

Khalil, A.A. 2013. Effect of climate change on evapotranspiration in Egypt. *Researcher,* 5(1), 7–12.

Kogan, F. and Guo, W. 2017. Strong 2015-2016 El Nino and implication to global ecosystems from space data. *International Journal of Remote Sensing,* 38(1), 161–178.

Kundzewicz, Z.W. 2008. Climate change impacts on the hydrological cycle. *Ecohydrological Processes and Sustainable Floodplain Management,* 2(4), 195–203.

Li, M., Zang, S., Zhang, B., Li, S. and Wu, C. 2014. A review of remote sensing image classification techniques: the role of spatio-contextual information. *European Journal of Remote Sensing,* 47, 389–411.

Li, X., Liu, L. and Huang, L. 2020. Comparison of several remote sensing image classification methods based on ENVI. *The International Archives of the Photogrammetry, Remote Sensing and Spatial Information Sciences,* 42(3), 605–611.

Liang, S. 2000. Narrowband to broadband conversions of land surface albedo I: algorithms. *Remote Sensing of Environment,* 76, 213–238.

Liu, W., Hong, Y., Khan, S.I., Huang, M., Vieux, B., Caliskan, S. and Grout, T. 2010. Actual evapotranspiration estimation for different land use and land cover in urban regions using Landsat 5 data. *Journal of Applied Remote Sensing,* 4, 041873, doi:10.117/1.3525566.

Ma, W., Hafeez, M., Ishikawa, H., and Ma., Y. 2013. Evaluation of SEBS for estimation of actual evapotranspiration using ASTER satellite data for irrigation areas of Australia. *Theoretical and Applied Climatology,* 112, 609–616.

Majozi, N.P., Mannaerts, C.M., Ramoelo, A., Mathieu, R., Mudau, A.E. and Verhoef, W. 2017. An intercomparison of satellite-based daily evapotranspiration estimates under different eco-climatic regions in South Africa. *Remote Sensing,* 9(307), doi:10.3390/rs9040307.

Marjani, S., Alizadeh-Choobari, O. and Irannejad, P. 2019. Frequency of extreme El Nino and La Nina events under global warming. *Climate Dynamics,* 53, 5799–5813.

Mason, S.J. 2001. El Nino, climate change, and Southern African climate. *Environmetrics,* 12, 327–345.

Mohad, H.I., Pakhriazad, H.Z. and Shahrin, M.F. 2009. Evaluating supervised and unsupervised techniques for land cover mapping using remote sensing data. *Malaysian Journal of Society and Space,* 5(1), 1–10.

Mohammadian, M., Arfania, R. and Sahour, H. 2017. Evaluation of SEBS algorithm for estimation of daily evapotranspiration using landsat-8 dataset in a semi-arid region of central Iran. *Open Journal of Geology,* 7, 335–347.

Muller, M. 2018. Cape Town's drought: Don't blame climate change. *Nature,* 559, 174–176.

Nasiri, V., Deljouei, A., Moradi, F., Sadeghi, S.M.M. and Borz, S.A. 2022. Land use and land cover mapping using Sentinel-2, Landsat-8 satellite images, and Google Earth Engine: a comparison of two composition methods. *Remote Sensing,* 14, 1977.

Nitze, I., Schulthess, U. and Asche, H. 2012. Comparison of machine learning algorithms random forest, artificial neural network, and support vector machine to maximum likelihood for supervised crop type classification. *Proceedings of the 4th GEOBIA,* 35–40.

Noi, P.T. and Kappas, M. 2017. Comparison of random forest, k-nearest neighbour, and support vector machine classifiers for land cover classification using Sentinel-2 imagery. *Sensors,* 18, doi:10.3390/s18010018.

Odongo, V.O., van Oel, P.R., van der Tol, C. and Su, Z. 2019. Impact of land use and land cover transitions and climate on evapotranspiration in the Lake Naivasha Basin, Kenya. *Science of the Total Environment,* 682, 19–30.

Palmer, A.R. and Weideman, C.I. 2011. Exploring trends in evapotranspiration in the KNP: towards a water use efficiency model for rangeland production in semi-arid savannas. *Proc. IXth International Rangeland Congress*, 2–8 April 2011, Rosario, Argentina.

Pandey, P.C., Koutsias, N., Petropoulos, G.P., Srivastava, P.K. and Dor, E.B. 2019. Land use/land cover in view of earth observation: data sources, input dimensions, and classifiers–a review of the state of the art. *Geocarto International,* 36(9), 957–988.

Philippon, N., Rouault, M., Richard, Y. and Favre, A. 2011. The influence of ENSO on winter rainfall in South Africa. *International Journal of Climatology,* 32(15), 2333–2347.

Rawat, J.S. and Kumar, M. 2015. Monitoring land use/cover change using remote sensing and GIS techniques: a case study of Hawalbagh block, district Almora, Uttarakhand, India. *The Egyptian Journal of Remote Sensing and Space Sciences,* 18, 77–84.

Rocha, S.M.G., Molinas, E., Rodrigues, I.S. and Neto, I.E.L. 2023. Assessment of total evaporation rates and its surface distribution by tridimensional modelling and remote sensing. *Journal of Environmental Management,* 327, 116846.

Rouault, M., & Pohl, B. and Penven, P. 2010. Coastal oceanic climate change and variability from 1982 to 2009 around South Africa. *African Journal of Marine Science,* 32, doi:10.2989/1814232X.2010.501563.

Rwasoka, D.T., Gumindoga, W. and Gwenzi, J. 2011. Estimation of actual evapotranspiration using the Surface Energy Balance System (SEBS) algorithm in the Upper Manyame catchment in Zimbabwe. *Physics and Chemistry of the Earth,* 36, 736–746.

Sazib, N., Mladenova, E. and Bolten, J.D. Assessing the impact of ENSO on agriculture over Africa using earth observation data. *Frontiers in Sustainable Food Systems,* 4, 509914.

Shamloo, N., Sattari, M.T., Apaydin, H., Kamran, K.V. and Prasad, R. 2021. Evapotranspiration estimation using SEBAL algorithm integrated with remote sensing and experimental methods. *International Journal of Digital Earth,* 14(11), 1638–1658.

Sheykhmousa, M., Mahdianpari, M., Ghanbari, H., Mohammadimanesh, F., Ghamisi, P. and Homayouni, S. 2020. Support vector machine versus random forest for remote sensing image classification: a meta-analysis and systematic review. *IEEE Journal of Selected Topics in Applied Earth Observations and Remote Sensing,* 13, 6308–6325.

Shikwambana, L. and Kganyago, M. 2023. Seasonal comparison of the wildfire emissions in southern Africa region during the strong ENSO events of 2010/11 and 2015/16 using trend analysis and anomaly detection. *Remote Sensing,* 15, 1073.

Shikwambana, L., Xongo, K., Mashalane, M. and Mhangara, P. 2023. Climatic and vegetation response patterns over South Africa during the 2010/2011 and 2015/2016 strong ENSO phases. *Atmosphere,* 14(2), 416.

Shirmohammadi-Aliakbarkhani, Z. and Saberali, S.F. 2020. Evaluating of eight evapotranspiration estimation methods in arid regions of Iran. *Agricultural Water Management,* 239, 106243, doi:10.1016/j.agwat.2020.106243.

Shoko, C., Dube, T., Sibanda, M. and Adelabu, S. 2015a. Applying the Surface Energy Balance System (SEBS) remote sensing model to estimate spatial variations in evapotranspiration in Southern Zimbabwe. *Transactions of the Royal Society of South Africa,* 70(1), 47–55.

Shoko, C., Clark, D., Mengistu, M., Dube, T. and Bulcock, H. 2015b. Effect of spatial resolution on remote sensing estimation of total evaporation in the uMngeni catchment, South Africa. *Journal of Applied Remote Sensing*, 9(1), doi:10.1117/1.JRS.9.095997.

Singh, R.K. and Senay, G.B. 2015. Comparison of four different energy balance models for estimating evapotranspiration in the midwestern United States. *Water,* 8(9), doi:10.3390/w8010009.

Sinha, P., Kumar, L. and Reid, N. 2012. Seasonal variation in land-cover classification accuracy in a diverse region. *Photogrammetric Engineering & Remote Sensing*, 78(3), 271–280.

Sisodia, P.S., Tiwari, V. and Kumar, A. 2014. A comparative analysis of remote sensing image classification techniques. *Institution of Electrical and Electronics Engineers*, 1418–1421.

Sobrino, J.A., Jimenez-Munoz, J.C. and Paolini, L. 2004. Land surface temperature retrieval from LANDSAT TM 5. *Remote Sensing of Environment*, 90, 434–440.

Su, Z. 2002. The surface energy balance system (SEBS) for estimation of turbulent heat fluxes. *Hydrology and Earth System Sciences*, 6, 85–99.

Talanow, K., Topp, E.N., Loos, J. and Martin-Lopez, B. 2021. Farmers perceptions of climate change and adaptation strategies in South Africa's Western Cape. *Journal of Rural Studies,* 81, 203–219.

Valipour, M., Sefidkouhi, M.A.G. and Raeini-Sarjaz, M. 2017. Selecting the best model to estimate potential evapotranspiration with respect to climate change and magnitudes of extreme events. *Agricultural Water Management*, 180, 50–60.

Veste, M., Littmann, T., Kunneke, A., Du Toit, B. and Seifert, T. 2020. Windbreaks as part of climate-smart landscapes reduce evapotranspiration in vineyards, Western Cape Province, South Africa. *Plant, Soil and Environment*, 66(3), 119–127.

Zhang, L., Dawes, W.R. and Walker, G.R. 2001. Response of mean annual evapotranspiration to vegetation changes at catchment scale. *Water Resources Research*, 37(3), 701–708.

Zhang, L., Hickel, K. and Dawes, W.R. 2004. A rational function approach for estimating mean annual evapotranspiration. *Water Resources Research*, 40, W02502, doi:10.1029/2003WR002710.

Zhang, K., Kimball, J.S. and Running, S.W. 2016. A review of remote sensing based actual evapotranspiration estimation. *WIREs Water*, 3, 834–853.

Zhao, J., Chen, X., Zhang, J., Zhao, H., and Song, Y. 2019. Higher temporal evapotranspiration estimation with improved SEBS model from geostationary meteorological satellite data. *Scientific Reports*, 9, 14981, doi:10.1038/s41598-019-50724-w.

Zwane, E.M. 2019. Impact of climate change of primary agriculture, water sources and food security in Western Cape, South Africa. *Journal of Disaster Risk Studies*, 11(1), doi:10.4102/jamba.v11i1.562.

APPENDIX ONE

The confusion matrices of each of the four LULC classifications were performed for the summer and winter seasons for the two years to determine the accuracy of the classification.

Summer 2015 SVM Confusion Matrix								
	Water	**Shrub**	**Grassland**	**Agriculture**	**Bareland**	**BuiltUp**	**Total**	**Users Accuracy**
Water	**97**	0	0	0	0	0	97	1.0000
Shrub	0	**90**	2	3	0	0	95	0.9474
Grassland	3	1	**95**	0	0	1	100	0.9500
Agriculture	0	7	4	**92**	0	2	105	0.8762
Bareland	0	0	0	4	**94**	1	99	0.9495
BuiltUp	0	1	0	1	6	**96**	104	0.9231
Total	100	99	101	100	100	100	**600**	0.0000
Producers Accuracy	0.9700	0.9091	0.9406	0.9200	0.9400	0.9600	0.0000	**0.9400**
Kappa Statistic	**0.9279988**							

Winter 2016 SVM Confusion Matrix								
	Water	**Shrub**	**Grassland**	**Agriculture**	**Bareland**	**BuiltUp**	**Total**	**Users Accuracy**
Water	**94**	1	0	0	1	2	98	0.9592
Shrub	0	**99**	7	0	1	3	110	0.9000
Grassland	2	1	**77**	0	0	8	88	0.8750
Agriculture	1	0	14	**100**	3	7	125	0.8000
Bareland	0	0	0	0	**95**	2	97	0.9794
BuiltUp	2	0	2	0	0	**78**	82	0.9512
Total	99	101	100	100	100	100	**600**	0.0000
Producers Accuracy	0.9495	0.9802	0.7700	1.0000	0.9500	0.7800	0.0000	**0.9050**
Kappa Statistic	**0.88599544**							

Summer 2020-21 SVM Confusion Matrix								
	Water	**Shrub**	**Grassland**	**Agriculture**	**Bareland**	**BuiltUp**	**Total**	**Users Accuracy**
Water	**96**	0	0	0	0	0	96	1.0000
Shrub	0	**94**	0	3	0	0	97	0.9691
Grassland	0	1	**94**	8	0	0	103	0.9126
Agriculture	0	5	3	**78**	11	2	99	0.7879
Bareland	0	0	0	3	**84**	1	88	0.9545
BuiltUp	4	0	3	8	5	**97**	117	0.8291
Total	100	100	100	100	100	100	**600**	0.0000
Producers Accuracy	0.9600	0.9400	0.9400	0.7800	0.8400	0.9700	0.0000	**0.9050**
Kappa Statistic	**0.886**							

Winter 2021 SVM Confusion Matrix								
	Water	**Shrub**	**Grassland**	**Agriculture**	**Bareland**	**BuiltUp**	**Total**	**Users Accuracy**
Water	**87**	0	0	0	6	3	96	0.9063
Shrub	10	**98**	1	1	0	0	110	0.8909
Grassland	1	2	**92**	17	2	3	117	0.7863
Agriculture	0	0	4	**77**	6	3	90	0.8556
Bareland	1	0	0	4	**71**	0	76	0.9342
BuiltUp	1	0	3	1	15	**91**	111	0.8198
Total	100	100	100	100	100	100	**600**	0.0000
Producers Accuracy	0.8700	0.9800	0.9200	0.7700	0.7100	0.9100	0.0000	**0.8600**
Kappa Statistic	**0.832**							

APPENDIX TWO

Seasonal variations in ET during the different climatic events and the normal year. The maps were all presented using the same scale or legend to highlight the influence of climatic events on seasonal ET.

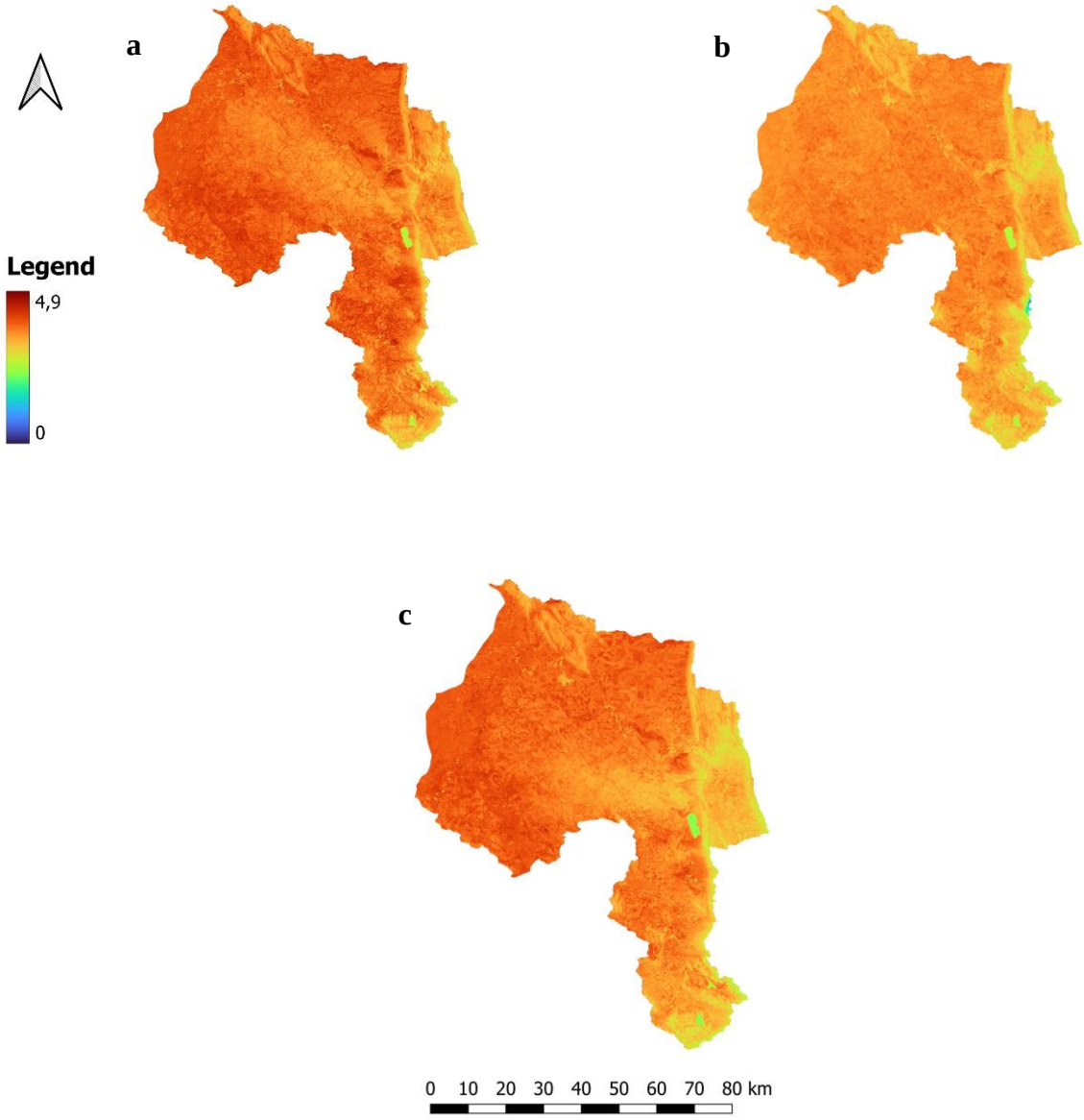

APPENDIX TWO A: SEBS derived ET rates for the summer seasons in the El Nino (2015-16) (a), normal (2019-20) (b) and La Nina (2020-21) (c) year

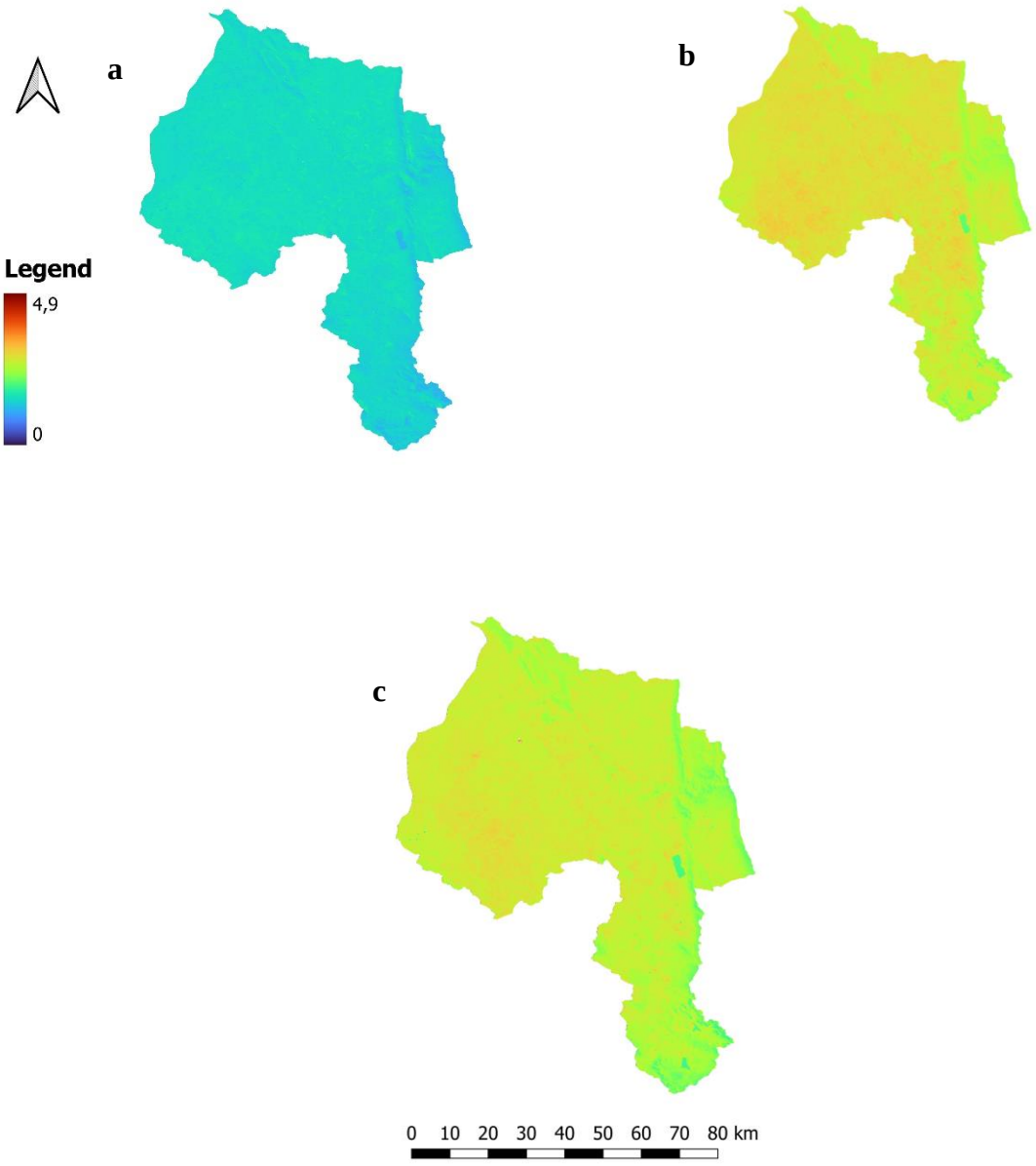

APPENDIX TWO B: SEBS derived ET rates for the autumn seasons in the El Nino (2015-16) (a)), normal (2019-20) (b)), and La Nina (2020-21) (c)) years.

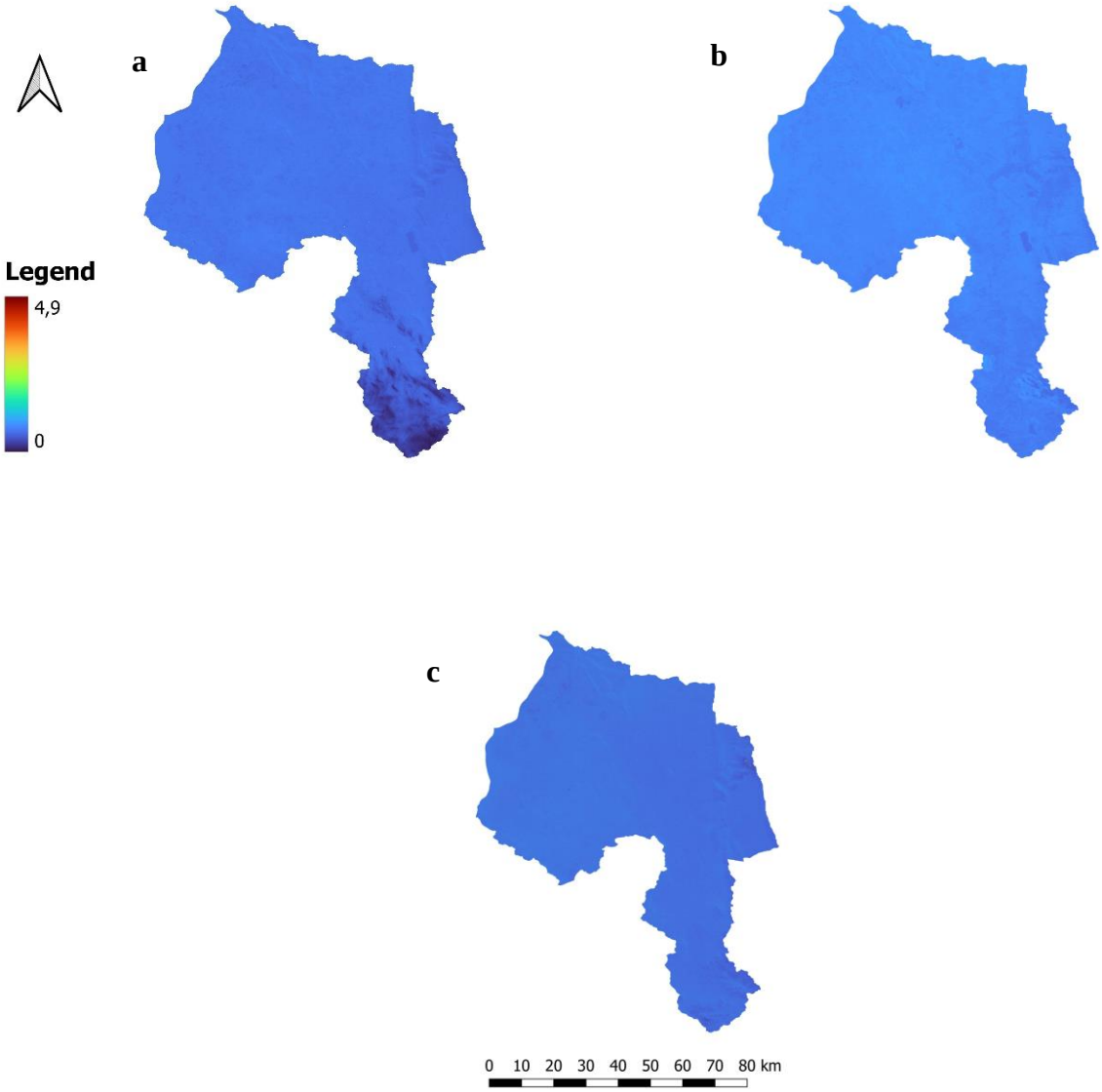

APPENDIX TWO C: SEBS derived ET rates for the winter seasons in the El Nino (2015-16) (a)), normal (2019-20) (b)), and La Nina (2020-21) (c)) years.

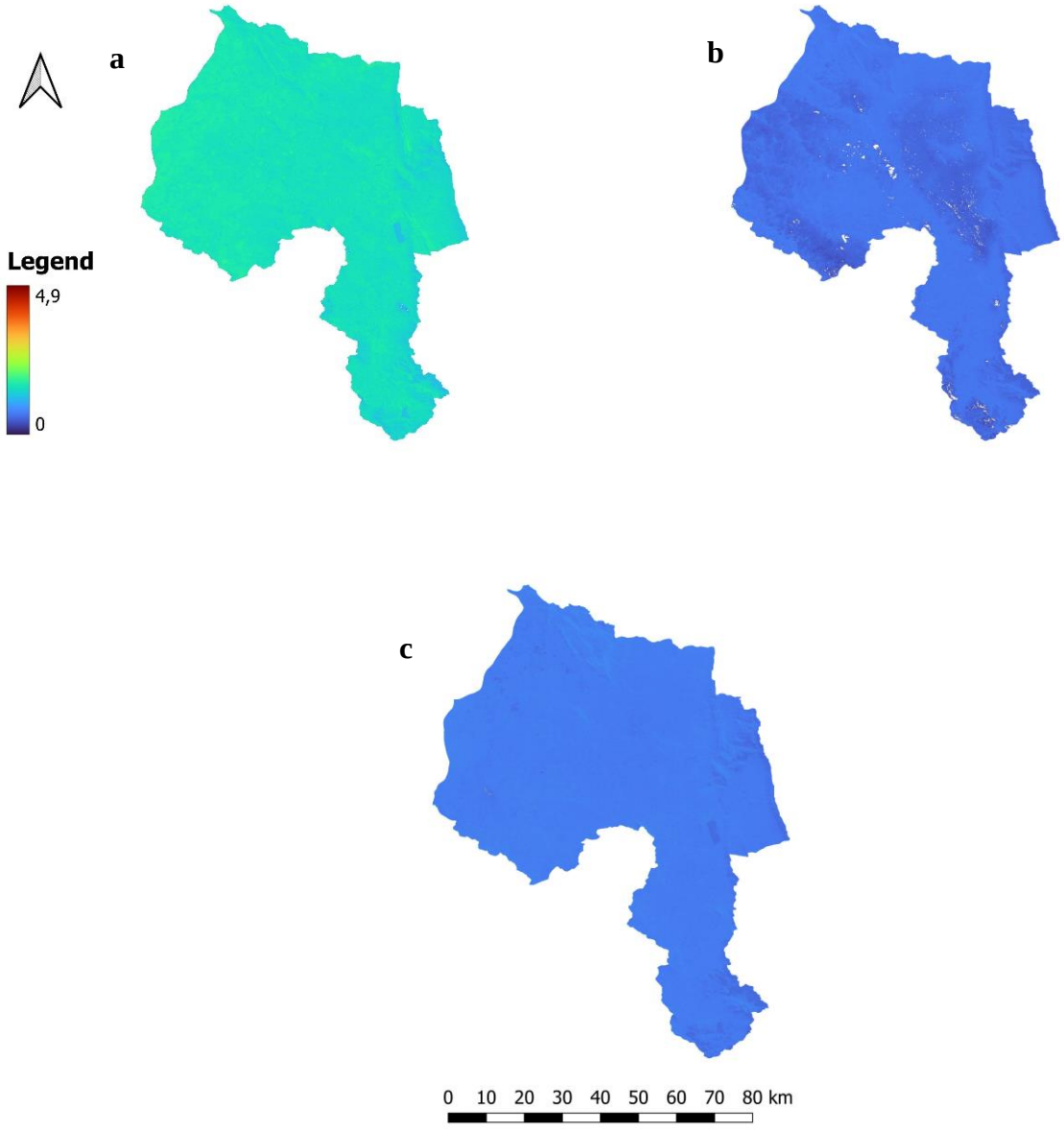

APPENDIX TWO D: SEBS derived ET rates for the spring seasons in the El Nino (2015-16) (a)), normal (2019-20) (b)), and La Nina (2020-21) (c)) years.